POLITECNICO DI TORINO

Master of Science in Materials Engineering For Industry 4.0

Master's Thesis

Study and the characterization of 3D printed sustainable plastic materials compared to injection molded ones



Supervisor

Prof. Massimo Messori S307939

Co-Supervisor

Prof.ssa Giovanna Colucci

Candidate

Mert Yüksel

ACADEMIC YEAR 2024/2025



Table of Content ACRONYMS......iv ABSTRACT......v 1.1. 1.1.1. 1.1.2. 1.2. TYPES OF THERMOPLASTICS10 1.2.1. 1.2.2. 1.2.3. 2. 2.1. 2.2. 2.2.1. 2.2.2. 2.2.3. 3.1. 3.1.1. 3.1.2. 3.1.3. 3.2. 3.2.1. 3.3. 3.3.1. 3.3.2. 3.3.3. Dynamic Mechanical Analysis41 3.3.4. 4.1. Characterization of Materials and Specimens44 4.1.1. Differential Scanning Calorimetry......44 4.1.2. Thermogravimetric Analysis50 4.1.3. 4.1.4. Tensile Test 57

ACRONYMS

ABS - Acrylonitrile Butadiene Styrene

AM – Additive Manufacturing

BPA – Bisphenol A

CAD – Computer-Aided Design

CLTE – Coefficient of Linear Thermal Expansion

DMA – Dynamic Mechanical Analysis

DSC – Differential Scanning Calorimetry

DTG – Derivative Thermogravimetry

FFF – Fused Filament Fabrication

GPO – General Purpose Output

ISCC PLUS - International Sustainability and Carbon Certification PLUS

ME – Mechanical Engineering

MPa – Megapascal

MVR - Melt Volume Rate

MWCNT – Multi-Walled Carbon Nanotube

PA – Polyamide

PEEK – Polyether Ether Ketone

PP – Polypropylene

STL – Stereolithography

Tg – Glass Transition Temperature

Tc – Crystallization Temperature

Tm – Melting Temperature

TGA – Thermogravimetric Analysis

UV – Ultraviolet

VOC – Volatile Organic Compound

VP – Vat Photopolymerization

ABSTRACT

The objective of this research was to evaluate the capability of additive manufacturing (3D printing) to fabricate polymer parts that are mechanically and thermally replicable to injection molded polymer components. Three recycled thermoplastic materials were reflected upon: Bayblend T85 X RE (PC/ABS blend), Eplon+ 6 IMP BK Q2A505 (PA6), and InnoEnd P1 M M112 BK (PP). As a primary objective of this work, a description on the structural integrity and thermal stability of parts produced via Fused Granular Fabrication (FGF) was evaluated against those of injection molded parts. For the comparison of the polymers in pellet and printed form, a series of material characterization tests were performed: Differential Scanning Calorimetry (DSC), Thermogravimetric Analysis (TGA), Dynamic Mechanical Analysis (DMA), and tensile testing.

Of all the materials that were tested, Bayblend T85 X RE was the only one to be successfully 3D printed, while PA6 and PP indicated major detachment and warpage due to their level of crystallinity and shrinkage tendencies. The DSC and DMA tests confirmed that Bayblend retained its amorphous structure and a glass transition around 125 °C after being printed, and the TGA test showed no evidence of thermal degradation under 450 °C. Tensile testing would show that the 3D printed Bayblend samples had stress at break mechanical strength similar to the reference injection molded samples but slightly lower due to inter-layer anisotropy.

Overall, the findings show that industrial-grade amorphous engineering polymers will achieve near injection molding mechanical and thermal performance with optimized parameters in 3D printing. Meanwhile, semicrystalline polymers like PA6 and PP are still not a cost-effective option for FGF 3D printing due to their poor dimensional stability. The findings demonstrate the potential for additive manufacturing as an ecofriendly alternative to conventional polymer processing, yet too many key aspects of the study highlight challenges faced.

INTRODUCTION

Sustainability is now an increasingly pressing area in production processes. In the case of plastic materials, it is becoming increasingly clear that new production methods will continue to target environmental impacts. Although plastics have a range of applications, long service life, and are of major importance in industry, fossil fuel-based production and low rates of plastics recycling present serious environmental challenges. Therefore, developing production processes that support the reduction of material loss as well as supporting a circular economy is critically important [1].

Recent developments in additive manufacturing (AM) technologies are providing a critical alternative for sustainable production. AM methods, especially through layer-by-layer production such as 3D printing, lead to less material waste than traditional manufacturing methods, and increase flexibility by enabling direct product production from digital designs. With reduced waste and optimized material use, 3D printing technologies have considerable potential for the production of sustainable plastic materials [2,3].

Injection molding, as a common practice, is a traditional method used in industry due to its efficiency in producing large volumes accurately. Injection molded plastic parts have high mechanical strength, homogeneous distribution of the materials, and repeatable surface quality, however, it has a few limitations. Injection molding comes with large amounts of initial costs, takes a long time for the mold to be produced, and manufacture loss [2]. 3D printing on the other hand is much more flexible, especially for low volume and custom productions, and also likely to generate less material waste than injection molding and use less energy than injection molding. Furthermore, tooling is eliminated, reducing the time and costs [3,4].

When it comes to sustainable plastic materials, both injection molding and 3D printing allow for the use of recycled polymers. However, when recycled plastics are reprocessed, the changes to the physical and chemical properties can present hurdles for production processes and the properties of the part. Recycled plastics may have different (lower) mechanical strength than virgin polymers and/or have different processing properties. The extent to which these materials deviate from virgin plastic can vary based on how they are extruded and the particularities of layered manufacturing [5].

This thesis contains four chapters. Chapter I is a general introduction to polymers, types and classifications of polymers, and most importantly, thermoplastics. Chapter II gives an introduction to AM, with a primary focus on thermoplastic materials. Chapter III presents the experimental work, including materials and methodology. Chapter IV presents the mechanical properties of the same materials through the processes of AM. The primary aim of this study is to comprehensively investigate and compare the mechanical and thermal properties of recycled polymer materials processed through two distinct manufacturing techniques: conventional injection molding and additive manufacturing (3D printing).

1. POLYMERS

Polymers are macromolecules that are made by joining together many kinds of smaller molecules called monomers. [6] The tremendous success of polymers is a result of their versatility and capacity to create materials, with various properties. Polymers are present in many items around us and serve a wide range of purposes in everyday life: apparel, footwear, cosmetics, furnishings, electrical and electronic devices, packaging materials, kitchenware, car components, coatings, inks, adhesives, tyres, among others polymers find extensive use in sectors such as automotive, aerospace, computing, construction, and numerous other applications due to their versatility and cost-effectiveness. [7]

1.1. Polymer Types

A monomer, which is a building block made up of carbon (C), oxygen (O), hydrogen (H), and nitrogen (N), is repeated to create polymers. [8]

Primary covalent bonds and secondary, or van der Waals, bonds are the two main forms of molecular bonds found in polymers. When two or more atoms share electrons from their respective valence shells, this is known as a covalent bond. In terms of secondary bonding, they are crucial for polymers. These bonds are far weaker than covalent bonds and are based on electrostatic interactions. [7]

Some of the primary polymer kinds can be conveniently described based on their characteristics and applications. The two primary categories into which they can be separated are thermosets and thermoplastics. [6]

Since this fundamental structural difference has a significant impact on material qualities, the names are also linked to each of their general thermal and processing characteristics in addition to their chemical structure. [7]

Other terms like "cross-linked" are occasionally used to refer to thermosetting polymers, respectively. Notably, the term "linear" here refers to molecular structure rather than mechanical (stress-strain) properties. [7]

It is appropriate to highlight the difference between cross-linked and linear polymers while synthesizing:

Cross-linked polymers: The main type of bonds are intrachain. Interchain bonds can be primary (covalent) or secondary. Network polymers (such as Bakelite, epoxy resins, or melamine-formaldehyde, which are highly cross-linked three-dimensional structures) are polymers that are extremely cross-linked.

Linear (or branched) polymers: Primary (covalent) bonds are found inside chains. Secondary interchain bonds are rendered ineffective or broken at high enough temperatures, allowing the various long chains to flow or move past one another with relative ease. "Branched chain" polymers are those composed of a linear main chain with smaller chains acting as branches of the main chain. [7]

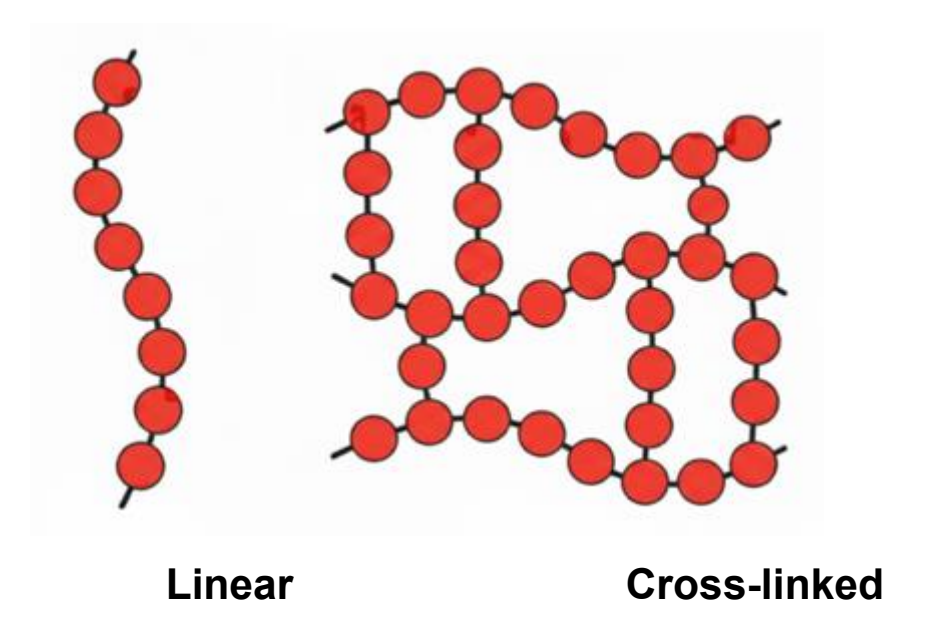


Figure 1.1 Chain topology of linear polymer and cross-linked polymers.

The structure of the chains in cross-linked and linear polymers differs, as seen in Figure 1.1.

Only a brief summary is provided because thermosetting polymers are outside of the focus of this work. However, the next sections will concentrate on the qualities, traits, and features of thermoplastic polymers.

1.1.1.Thermosetting Polymers

Thermosetting polymers, also known as thermosets, are a class of polymers distinguished by the property that, when heated, they transform from a liquid solution into a solid material permanently. In this regard, they behave differently from thermoplastic polymers, which, with few exceptions, exhibit a reversible solid-to-liquid transition upon heating to a comfortable temperature. The end products are also known as thermosetting polymers, even though the irreversible liquid-to-solid transition can also be created by other techniques including UV or electron beam irradiation. The phrase "cure of the material" generally implies the process whereby the liquid solution begins to become solid. The more important component of the initial liquid solution is often a collaboration of comonomers that can react with one another when stimulated by external factors such as heat or UV light. [9]

Thermosets are different from thermoplastics since they include cross-linked polymer chains, which are connected by strong covalent bonds. Thermosets are insolublebecause they are cross-linked; meanwhile, if heated one, it would undergo chemical degradation. cross-link This behavior is due to the presence of cross-links, which restrict molecular motion. However, not all cross-linked polymers are brittle; for example, vulcanized rubber remains elastic because it contains only a limited number of cross-links. In contrast, highly cross-linked thermosets cannot flow because chain sliding is inhibited, unlike in linear or branched thermoplastic polymers. Thermosets

reach a state of polymerization and cross-linking in a curing phase that typically involves a hardener and heating or promoter. Thermosets initially behave like a viscous fluid. Thermosets go from a viscous fluid to a rubbery gel (a viscoelastic material), and onto a glassy solid as they cure. If thermosets are heated after curing, they become soft and extensible at elevated temperatures.

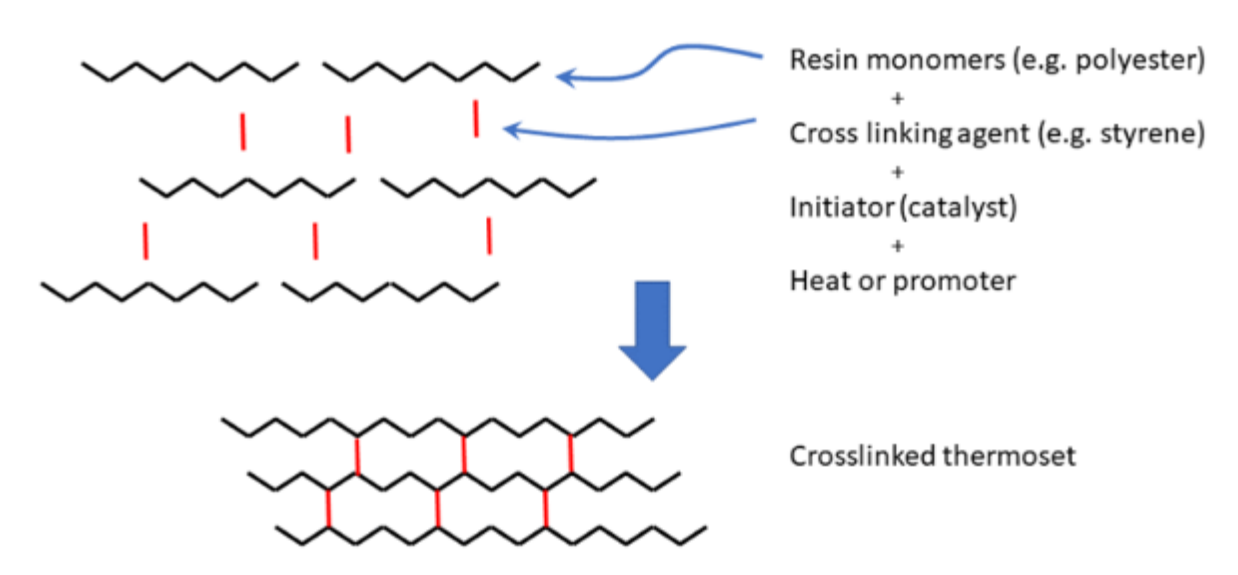


Figure 1.2 Illustration of the molecular cross-link formation for a thermoset polymer.

As indicated in Figure 1.2, thermoset resins are frequently divided into two components: part A, which is the resin, and part B, which is the cross-linking curing agent, also known as the hardener. Thermoset resins are frequently divided into two components: part A, which is the resin, and part B, which is the cross-linking curing agent (also known as the hardener); however, this is not always the case, as some systems use a resin combined with an initiator, which functions differently from a hardener. The synthesis between these two substances through a chemical reaction is known as the "curing reaction" or "curing process."

1.1.2. Thermoplastic Polymers

Thermoplastics are macromolecular structures which are chemically autonomous. They harden when cold and soften or melt when heated, leading to reformation. Thermoplastics can be recycled and/or reprocessed multiple times, and can be heated and cooled multiple times without major consequences to their molecular or chemical structure. Thermoplastics can also be blended with fillers or additives to improve their mechanical and rheological properties. [10]

Advantages

- Welding and thermoforming are allowed because heating softens or melts.
- Processing cycles are much shorter than either thermoset material because there is no chemical reaction due to cross-linking.
- Processing is much easier to control with only a physical transformation to monitor.
- When properly dried prior to processing, thermoplastics do not emit gases or water vapor.
- The waste can be used to the extent of the virgin matter since physical softening or melting are reversible. [11]

Disadvantages

- As the temperature increases, the modulus retention decreases due to the lack of permanent chemical links between macromolecules.
- For this reason, both the creep and relaxation behaviors are not as favorable as for the thermosets.
- In a fire, fusibility favors dripping and obliterates final residual physical cohesion.
- There are few materials that can be worked in the liquid state. [11]

Semi-crystalline polymers

Several typical polymers are classified as semi-crystalline. Polymers are found in both crystalline and amorphous states. Semi-crystalline has a crystallinity, which affects the properties, of between 10% to 80%. It is not possible for a distribution of polymer chains to be 100% crystallized. Semi-crystalline polymers do display defined melting temperatures and unorganized molecular forms. The material converts heat and goes into a liquid of high viscosity with a defined increase in temperature instead of gradual melting. Semi-crystalline polymers have both a glass transition (Tg) and melting temperature (Tm). [10]

Amorphous polymers

Amorphous polymers are chains of polymers that have anisotropic and a non-uniform molecular orientation. For shorter chains, the molecular orientation of this polymer may be regular. By gradually heating the amorphous polymer, which is a thermoplastic, you will change the state from a stiff or glass-like state to a rubber state, until it becomes molten. The term "glass transition temperature" (Tg) refers to glass-rubbery state transition. Amorphous polymers have a molecular structure that is exclusively random and only shows glass transition (Tg). Semi-crystalline thermoplastics are opaque/translucent, while amorphous thermoplastics generally are transparent. [10] Figure 1.3 illustrates the amorphous and semi-crystalline structures.

Semi-crystalline Amorphous Amorphous

Figure 1.3 Semi-crystalline polymers (left) contain sections of ordered structure, while amorphous polymers (right) have an unorganized structure.

The ordered molecular structure of crystallinity has the behavior of melting at a predetermined temperature. Because of this, the semi-crystalline polymers polyethylene, polyacetal, and nylon will exhibit a noticeable melting transition, and have a melting point (Tm). The amorphous polymers such as polystyrene, polycarbonate, and poly(phenyl sulfone), do not actually melt, but rather soften above the glass transition temperature (Tg). This behavior is illustrated by the differential scanning calorimetry (DSC) thermograms presented in Figure 1.4.

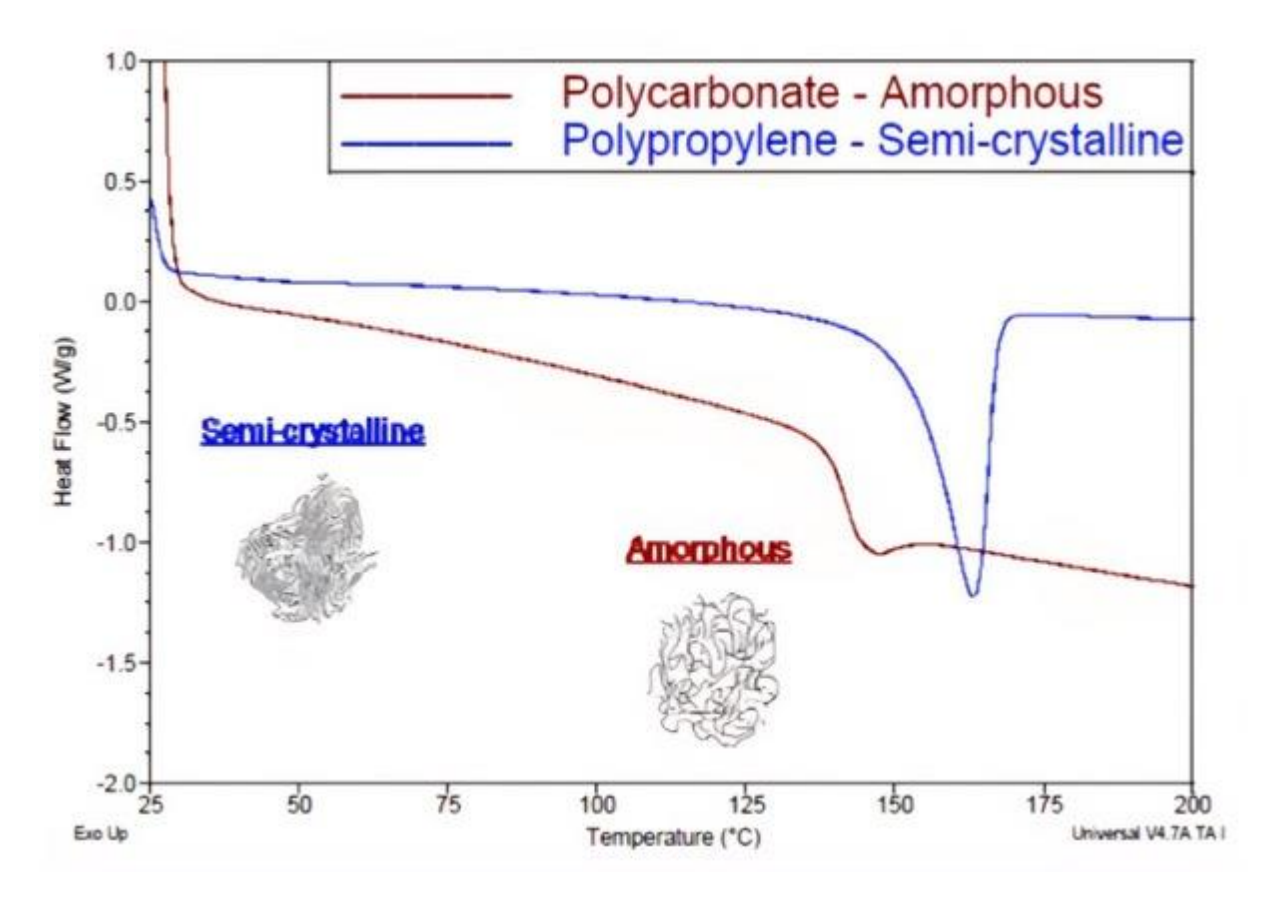


Figure 1.4 Differential scanning calorimetry thermogram demonstrating an amorphous polymer's glass transition (red curve) and a semi-crystalline polymer's melting transition (blu curve).

The difference in molecular arrangement between semi-crystalline and amorphous also has consequences in mechanical properties, particularly with respect to temperature dependence. As a rule of thumb, amorphous plastics exhibit a relative modulus consistency over a temperature range. However, as the temperature reaches the glass transition temperature, a sharp decrease will take place. In contrast, semi-crystalline polymers will have modulus stability below the glass transition temperature, which in most cases will be subambient, and will then steadily decrease from the glass transition temperature to melting point. This is shown in Figure 1.5.

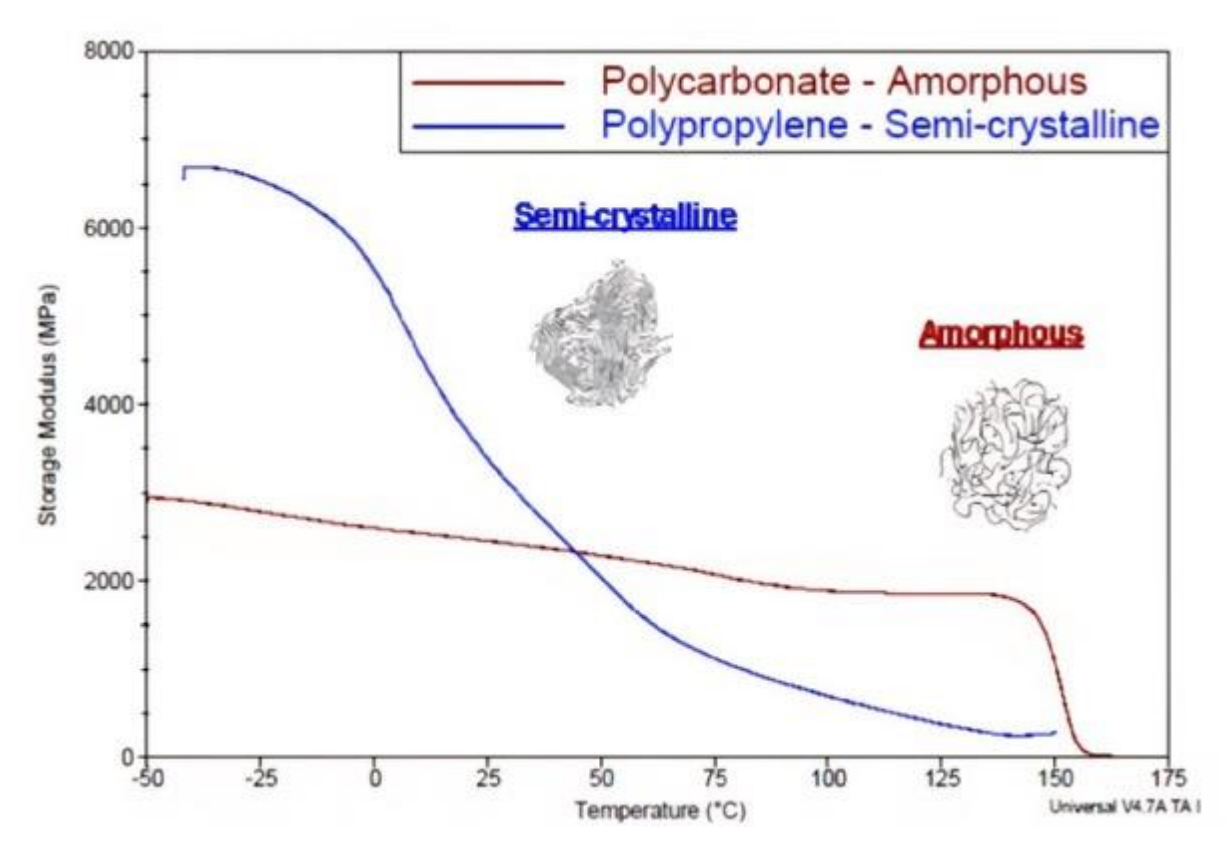


Figure 1.5 Dynamic mechanical analysis (DMA) thermogram depicting the temperature dependence of the storage modulus for both semi-crystalline and amorphous polymers.

Due to their viscoelastic nature, polymeric materials respond to time and temperature in a similar manner, allowing temporal changes to be inferred from their thermal stability.

Different semi-crystalline and amorphous polymers are listed in Figure 1.6.

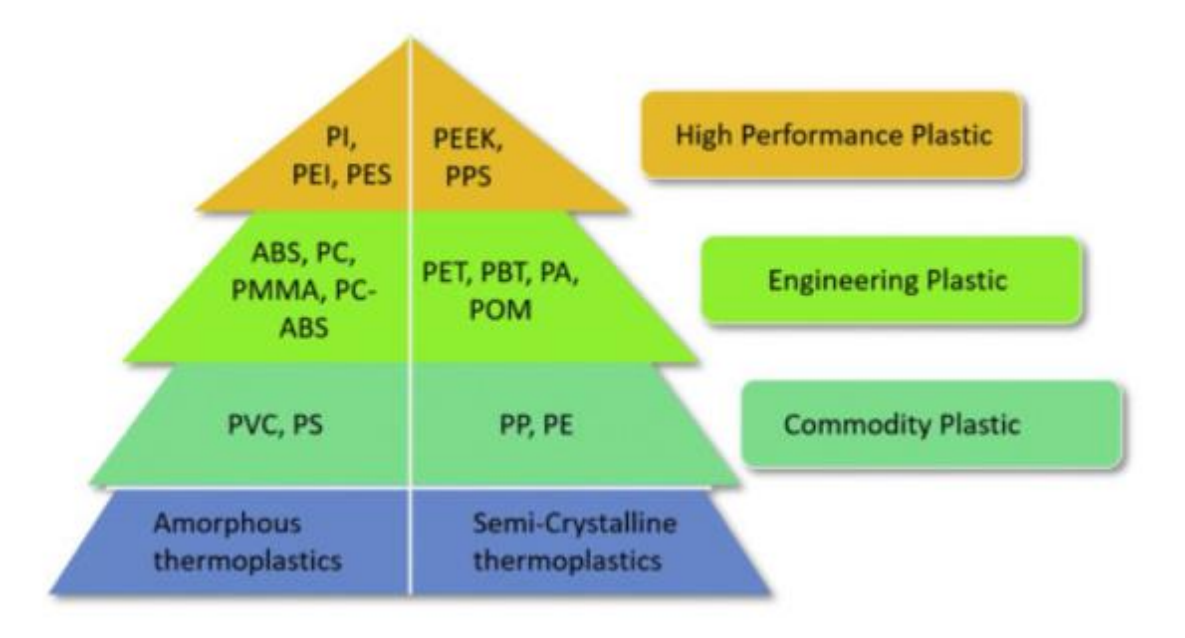


Figure 1.6 Thermoplastics available for different applications.

High Performance Plastic

PI: Polyimide

PEI: Polyetherimide

PES: Polyethersulfone

PEEK: Polyetheretherketone

PPS: Poly(phenylene sulfide)

Engineering Plastic

ABS: Acrylonitrile Butadiene Styrene

PC: Polycarbonate

PMMA: Poly(methyl methacrylate) (Also commonly known as Acrylic)

PC-ABS: Polycarbonate / Acrylonitrile Butadiene Styrene Blend (Alloy)

PET: Poly(ethylene terephthalate)

PBT: Poly(butylene terephthalate)

PA: Polyamide (Commonly known as Nylon)

POM: Polyoxymethylene (Also known as Acetal or Polyacetal)

Commodity Plastic

PVC: Poly(vinyl chloride)

PS: Polystyrene

PP: Polypropylene

PE: Polyethylene (Includes variations like HDPE, LDPE)

1.2. TYPES OF THERMOPLASTICS

According to applications and uses, thermoplastics can be classified into categories;

- Commodity plastics
- Engineering plastics
- High performance plastics

1.2.1. Commodity plastics

Commodity plastics are produced on a large scale for common use, though they generally do not offer excellent mechanical properties. They are inexpensive, however, and their mechanical properties are not good. These types of plastics are typically used for photo films, trash cans, beverage bottles, and packaging films. Polystyrene (PS), polypropylene (PP), polyethylene (PE), and poly(vinyl chloride) (PVC) are all considered commodity plastics. [10] The commodity plastic in this study is explained below.

Polypropylene (PP)

Polypropylene is a semicrystalline, stiff thermoplastic that finds extensive use in common products such as medical gadgets, household goods, and packaging trays. The degree of crystallinity, crystalline shape, and orientations of PP can all be used to identify its properties. PP is one of the least expensive plastics on the market. In Table 1.1, the mechanical properties of PP are explored. [10] The molecular structure of PP is illustrated in Figure 1.7.

Property	Typical Value
Density (g/cm³)	1.04–1.06
Tensile Strength (MPa)	31–45
Strain at Break (%)	50
Tensile Modulus (GPa)	1.5–3
Printing Temperature (°C) (Injection)	230–260
Melting Temperature (°C)	160 ± 10

Table 1.1 Typical properties of polypropylene material.

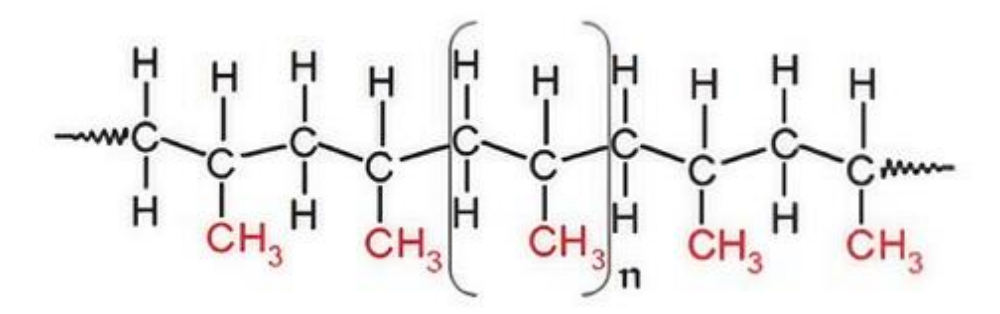


Figure 1.7 The molecular structure of PP.

1.2.2. Engineering plastics

Engineering plastics are produced for mechanical strength, chemical resistance, and high thermal characteristics unlike commodity plastics. When combined, commodity plastics and engineering plastics may have very similar uses from industrial parts to home uses. Examples of engineering plastics are ABS, polycarbonate (PC), poly(methyl methacrylate) (PMMA), poly(ethylene terephthalate) (PET), poly(butylene terephthalate) (PBT), polyamide (PA), polyoxymethylene (POM), etc. Engineering plastics in this study are explained below.

Acrylonitrile butadiene styrene (ABS)

Acrylonitrile butadiene styrene (ABS) is an engineering plastic consists of a styrene-acrylonitrile copolymer and a butadiene-styrene copolymer (synthetic rubber) created a glassy matrix structure. ABS has the best properties when the glassy and rubbery phases are optimized for application. ABS copolymers exhibit toughness, good thermal stability, and significantly improved performance over polystyrene plastics. ABS copolymers cover a range of applications including automotive, household and furniture, and toys. The mechanical properties of ABS are found in Table 1.2 [10], and its molecular structure is shown in Figure 1.8.

Property	Typical Value
Density (g/cm³)	1.03
Tensile Strength (MPa)	32
Strain at Break (%)	9
Tensile Modulus (GPa)	1.8
Printing Temperature (°C) (Injection)	220–240
Melting Temperature (°C)	245 ± 10

Table 1.2 Typical properties of ABS material.

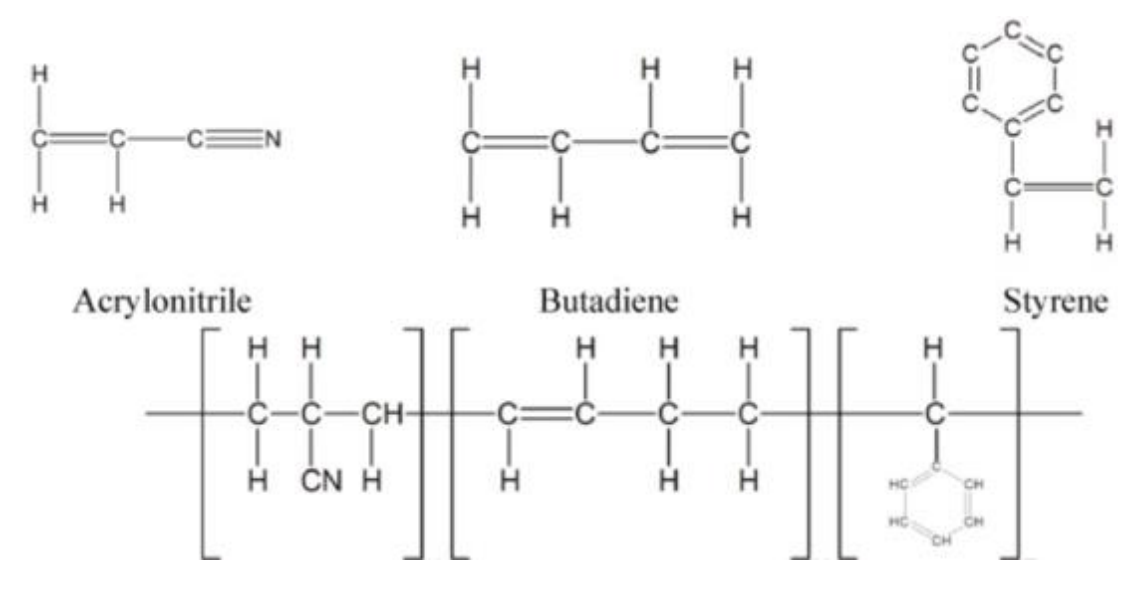


Figure 1.8 Molecular structure of Acrylonitrile Butadiene Styrene.

Polyamide (PA)

Polyamide (PA) (also known as NylonTM) is an engineering plastic that is being converted to mechanical application due to its rigidity, load capacity, and mechanical properties. PA is a straightforward material to machine and finish which is why it is being converted to replace metals like bronze, brass, and aluminum in different industries and agricultural applications. Unfortunately, PA does absorb moisture; this absorption could change its dimensions, so it is not recommended for water application. PA can come in a variety of types; PA 6, PA 12, PA 66, PA 69, and PA 46. The numerical codes in polyamide designations indicate the number of carbon atoms present in the monomer units forming the polymer chain. For polyamides derived from a single monomer (such as lactams or amino acids), the number refers to the number of carbon atoms in that monomer; for example, PA 6 is produced from caprolactam, which contains six carbon atoms, and PA 12 from laurolactam, which contains twelve carbon atoms. In contrast, for polyamides synthesized from two different monomers one diamine and one diacid—the first and second numbers represent the number of carbon atoms in the diamine and diacid, respectively. For instance, PA 66 is formed from hexamethylenediamine (six carbons) and adipic acid (six carbons), PA 69 from hexamethylenediamine (six carbons) and azelaic acid (nine carbons), and PA 46 from tetramethylenediamine (four carbons) and adipic acid (six carbons). The mechanical properties of PA are in Table 1.3. [10] The molecular structure of PA 6 and the synthetic routes are illustrated in Figure 1.9.

Property	Typical Value
Density (g/cm³)	1.13
Tensile Strength (MPa)	66.5

Property		Typical Value
Compressiv	ve Strength (MPa)	68
Strain at Break (%)		210
Tensile Mod	dulus (GPa)	2.4
Printing (Injection)	Temperature	(°C) _{250–270}

Table 1.3 Typical properties of PA 6 material.

Figure 1.9 Synthetic routes to polyamide 6.

Polycarbonate (PC)

Polycarbonate (PC) is an amorphous engineering thermoplastic that has excellent impact resistance, optical clarity, and broad temperature resistance range as a result of the carbonate ester bonds between the bisphenol A units. PC has high tensile and flexural strength, dimensional stability and impact resistance even at low temperatures. PC has limited scratch resistance and limited ultraviolet (UV) radiation resistance, which is typically addressed through surface coatings or additives. Because of these properties PC is often used in automotive items, optics or protective equipment. [12] The mechanical properties of PC are in Tabe 1.4. The molecular structure of PC and the synthetic route are illustrated in Figure 1.10.

Property	Typical Value
Density (g/cm³)	1.20
Tensile Strength (MPa)	60
Strain at Break (%)	60
Tensile Modulus (GPa)	2.2
Printing Temperature (°C) (Injection)	260–300
Melting Temperature (°C)	220–230

Table 1.4 Typical properties of PC material.

HO
$$\stackrel{\text{CH}_3}{\longrightarrow}$$
 OH + CI-C-CI $\stackrel{\text{O}}{\longrightarrow}$ 1 O $\stackrel{\text{CH}_3}{\longrightarrow}$ O-C $\stackrel{\text{CH}_3}{\longrightarrow}$ + 2 H₂O + 2 NaCI

Figure 1.10 The molecular structure and the synthetic route of PC.

Acrylonitrile Butadiene Styrene/Polycarbonate blend

ABS/PC blends offer a unique combination of properties from both polymers [13]. The addition of ABS improves the melt flow characteristics of PC, which makes it easier to process large thin-walled parts. The addition of ABS also improves the impact resistance of PC, particularly at low temperatures, while preserving the material properties for high strength and stiffness. ABS/PC blends also exhibit desirable UV resistance, good dimensional stability at ambient temperatures and at elevated temperatures, as well as halogen-free flammability qualities [14]. ABS/PC was first commercially introduced in 1971 by BorgWarner (now Sabic Innovative Plastics) under the name CycoloyTM. In 1977 Bayer (now Mobay) introduced PC/ABS under the name Bayblend through a license agreement with BorgWarner. Today PC/ABS blends are widely used in the automotive interior and exterior parts, desktop and laptop computers, copiers, printers, telecommunications equipment, electrical devices, and household appliances. The mechanical properties of ABS/PC are in Table 1.5. The molecular structure of ABS/PC is illustrated in Figure 1.11.

Property	Typical Value
Density (g/cm³)	1.10 – 1.20
Tensile Strength (MPa)	45 – 60
Strain at Break (%)	20 – 60
Tensile Modulus (GPa)	2.0 – 2.4
Printing Temperature (°C) (Injection)	240 – 270
Melting Temperature (°C)	230 – 260

Table 1.5 Typical properties of ABS/PC material.

$$\begin{array}{c}
CH_3 \\
C \longrightarrow C \longrightarrow C \longrightarrow C
\end{array}$$

$$\begin{array}{c}
CH_3 \\
C \longrightarrow C \longrightarrow C
\end{array}$$

$$\begin{array}{c}
C \longrightarrow C$$

$$\begin{array}{c}
C \longrightarrow C
\end{array}$$

$$\begin{array}{c}
C \longrightarrow C
\end{array}$$

$$\begin{array}{c}
C \longrightarrow C$$

$$C \longrightarrow$$

Figure 1.11 The molecular structure of ABS/PC, a) PC b) ABS

1.2.3. High-performance plastics

Certain plastic materials are utilized in some high-performance applications that provide superior properties than those of the common materials. Below is one of the advanced engineering plastics.

Pol(yether ether ketone) (PEEK)

Poly(ether ether ketone) (PEEK) is a semicrystalline thermoplastic with extraordinary mechanical, chemical, rheological and electrical properties compared to regularly used plastics, which allow its use in a variety of applications, including biomedical implants, wear-resistant parts, and parts requiring thermal stability. While PEEK is relatively expensive, many studies have investigated PEEK based composites for specific applications. With remarkable thermal stability, PEEK can be used continuously at temperatures above, and in some instances approaching, 250 °C for long periods of time. It also has excellent flame resistance, producing relatively low-levels of gases while burning, and high resistance to x-rays/beta/gamma radiation. These properties make PEEK composites well-suited for fabrication of parts for industrial applications requiring high temperature stability or aerospace/satellite parts and components. Various additives used within the PEEK matrix for such applications are shown in Table 1.6. [10]

PEEK Composite	Result / Effect
PEEK / MWCNT(Multi-Walled Carbon Nanotube)	Improved impact and tensile strength, but reduced failure strain
PEEK / Carbon fiber	Enhanced flexural strength and interlaminar shear strength
PEEK / Nano diamond particle	Increased thermal conductivity

PEEK Composite	Result / Effect	
PEEK / Pitch-based fiber	carbon Higher crystallinity	

Table 1.6 Different PEEK composites and corresponding effects.

PEEK represents a highly promising material, but there are some issues that need attention during 3D printing. Specifically, the build-up of high thermal stresses during processing can lead to warpage and interlayer delamination, adversely affecting dimensional accuracy and mechanical performance [10]. Table 1.7 summarizes the mechanical properties of PEEK. And the molecular structure of PEEK is illustrated in Figure 1.12.

Property	Typical Value
Density (g/cm³)	1.3
Melting temperature (°C)	343
Glass transition temperature (°C)	143
Coefficient of thermal expansion (ppm/K)	Below Tg: 55 Above Tg: 140
Heat deflection temperature (°C)	152
Thermal conductivity (W/m·K)	0.32
Young's modulus (GPa)	4
Tensile strength (MPa)	100
Elongation at break (%)	45
Flexural modulus (GPa)	3.9
Flexural strength (MPa)	162
Compressive modulus (GPa)	3.2
Compressive strength (MPa)	125
Hardness (Shore D)	84.5
Water absorption (%)	0.45

Property	Typical Value	
Flammability	V-0	

Table 1.7 Typical properties of PEEK material.

$$F - \begin{array}{c} & & \\ &$$

Figure 1.12 The molecular structure and the synthetic route of PEEK.

2. ADDITIVE MANUFACTURING

2.1. Introduction to Additive Manufacturing

In the 1980s, AM technology was first used to create rapid and functional prototypes from various materials [15,16]. It is now being adopted in many sectors of manufacturing and replacing traditional manufacturing processes, because of its ability to create geometrically complex and lightweight designs with high mechanical performance [16]. Commonly referred to as 3D printing, AM technology can fabricate metallic, polymeric, ceramic, and composite components under delicately controlled conditions with complex geometric designs, by depositing material layer-by-layer from computer-aided design (CAD) data [17,18]. AM is a process that allows for customized, low-volume manufacturing while offering considerable design freedom [16].

Compared to traditional composite manufacturing methodologies, AM technology offers distinct advantages in the rapid manufacturing of customized parts with complex geometric designs, reduced material use, and no additional tooling [19]. In addition, AM has been demonstrated as an environmentally sustainable technology, which can reduce global carbon dioxide emissions by 525.5 Mt by 2025 [18]. From a product development perspective, AM processes can reduce costs up to 70% and time to market up to 90% [18].

A key benefit of AM is its near-constant manufacturing cost, which is mostly unaffected by volume of production and product complexity. Also, AM is relatively more environmentally friendly than traditional methods, with less waste generation, justifying a stronger plan for sustainable manufacturing [18]. AM has a clear advantage in cases of low volume production with an emphasis on design realization and functionality rather than cost [17] (see Figure 2.1).

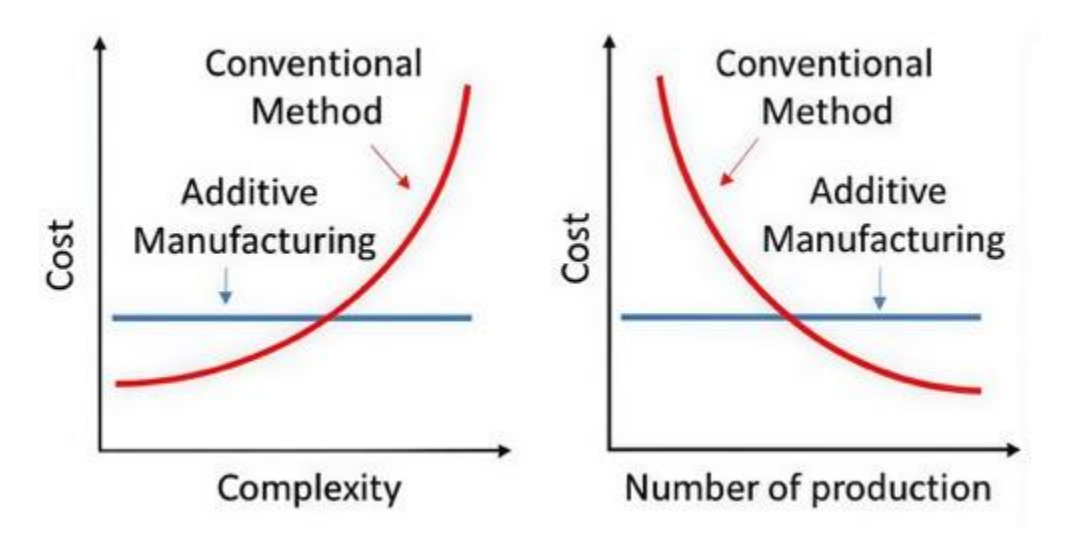


Figure 2.1 A comparison between AM and conventional manufacturing methods in terms of cost, design complexity, and production volume. [16]

2.2. Additive Manufacturing Technologies for Polymers

Polymers and their composites are some of the most popular materials in AM because of their natural lightweight and the multiple mechanical, thermal, electrical, fire retardant and biocompatible properties that can be fabricated in printed parts [18]. Examples of polymeric materials used in AM include viscous polymer inks, thermoplastic powders and filaments, as well as photocurable thermosetting resins. The potential applications of polymers and their composites are limitless and include fields as diverse as biomedical engineering, aerospace, automotive, electronics, soft robotics, energy, environmental technology and cultural [18].

AM was originally developed as a rapid prototyping method for demonstration purposes. With the increasing applications of AM technology for the manufacturing of end-use parts, it has become apparent that one of the many challenges is the limited number of materials that can be processed. Given the necessary materials often did not have essential properties like thermal and electrical conductivity, biocompatibility, and high mechanical strength, AM materials are generally not suitable to replace material parts. A significant amount of effort has therefore been invested into the research and development of new materials in the last decade for the AM of polymers. At the same time, AM systems continue to be improved in order to provide better accuracy, speed, and resolution [18].

Material extrusion (ME) is the primary AM technique for polymers. It involves heating thermoplastic material and forcing it through a nozzle, laying down material layer by layer to construct the part. While the nozzle moves back and forth in a lateral direction to define the part geometry, the build platform moves vertically after each layer is completed. This is also recognized as fused filament fabrication (FFF) and primarily uses thermoplastic polymers in filament form as its feedstock [20]. A schematic representation of the ME process is shown in Figure 2.2, which corresponds to the process widely referred to in the literature as fused deposition modeling (FDM); FFF is the term commonly used in academic and open-source contexts, whereas FDM is the trademarked designation of Stratasys.

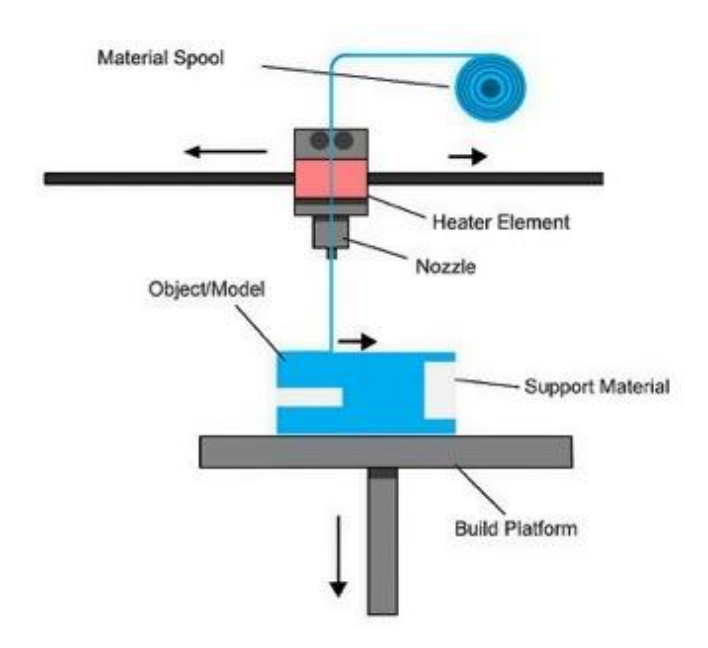


Figure 2.2 A schematic representation of the FFF process.

2.2.1. Fused Deposition Modeling (FDM)

ISO/ASTM standards divide AM technology into seven different categories [21]. The technology of material extrusion is one of these. Crump developed material extrusion in 1988, and it became commercially available in 1990 under the title FDM (Fused Deposition Modeling) [22]. Since then, low-volume part manufacturing, conceptual and functional prototypes, and product development have all made use of FDM technology. The application of AM technology has grown quickly in industries like design, healthcare, education, automotive, and aerospace because of its benefits [23-25].

FDM is based on feeding a thermoplastic filament through an active nozzle that applies heat to the filament and every section of the filament will be released layer by layer based on rendering (cross-sectional slices) of a 3D CAD model [26]. Because the parts are manufactured layer by layer, their overall shape will have various degrees of surface roughness and have a visible stair-stepped appearance. The surface roughness will affect how visually appealing and mechanically strong the printed part from the FDM process, but will depend on the intended application.

There are many process variables that contribute to the quality of FDM printed parts. These variables consist primarily of extrusion temperature and speed, layer height, part position, support structures required, and ambient conditions in the build chamber. The FDM printing process will need to be modified based on the specifications required by the material being used if you are going to create smooth surfaces with structurally sound parts.

Another aspect of FDM that is important to note is the anisotropic properties of the printed parts. That is, the mechanical characteristics of the printed materials can differ based on the direction of the printed part. Therefore, it is important to define the build orientation based on how the part will be used in an application [27].

FDM technology enables access to a wide variety of materials, including but not limited to the common polymers ABS, and poly(lactic acid) (PLA), as well as high-performance thermoplastics, such as poly(ether ketone ketone) (PEKK), polyethereimide (PEI), poly(phenyl sulfone) (PPSU), and PC, which are suitable for applications requiring high mechanical strength and thermal resistance. The availability of these advanced materials is one of the reasons that FDM has been able to grow so quickly in a myriad of industrial sectors [28].

FDM technology is an AM process whereby a thermoplastic filament is melted to a viscous state passing through an extruder that is mounted to a system that can move in the XYZ Cartesian axes. The melted material is deposited in a controlled way that matches the geometry of each sliced layer of the digital 3D model created. Once a layer is finished printing, the build platform will drop equal to the height of one layer, permitting the next layer to be printed on top of the previous layer. This is repeated layer by layer until the 3D model has been made [22,26]. A schematic to show the system is shown in Figure 2.3.

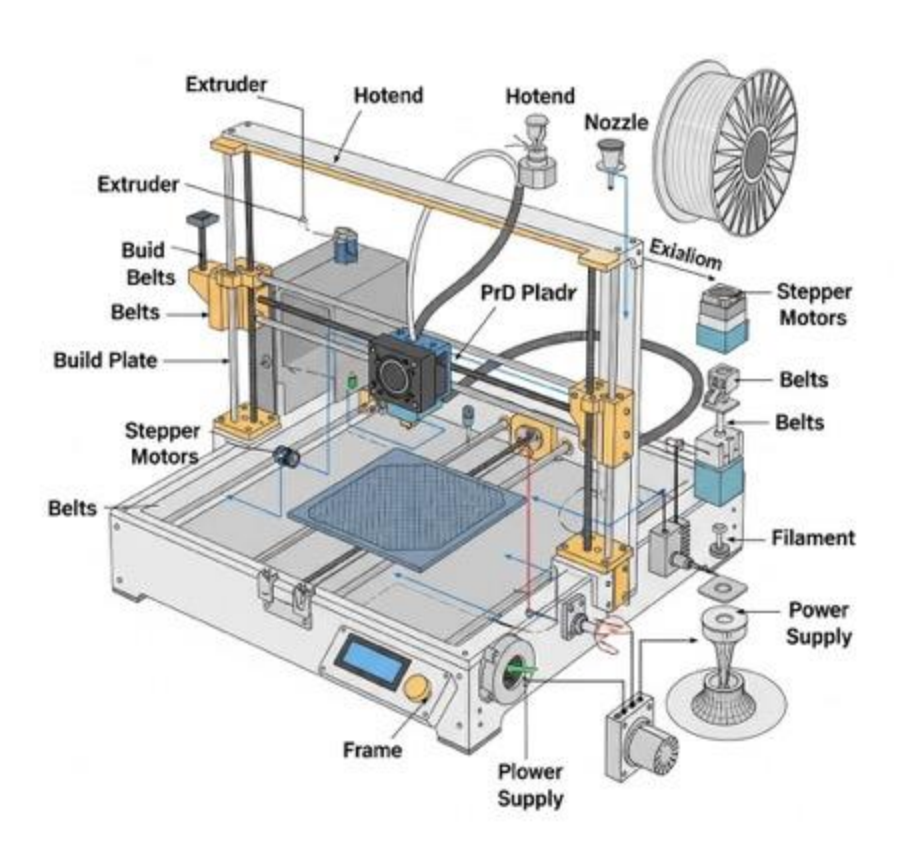


Figure 2.3 Schematic representation of FDM (Fused Deposition Modeling).

To produce high-strength parts with little surface roughness or defects, one must consider a number of parameters on the basis of the part's geometry. This includes the

appropriate layer thickness, in a valid position on the build platform, in the best orientation, appropriate toolpaths, and supporting additional structures where needed.

During 3D printing, it is important to set the extrusion temperature, extrusion rate, and print head speed, since these parameters will affect the quality of each printed layer [22, 29].

Figure 2.5 displays a schematic of a typical toolpath used in an FDM system. In applying proper toolpath strategies parts can be fabricated using partial infills. This allows parts to be built hollow, and non-functional display models. This reduces the volume of material consumed [22].

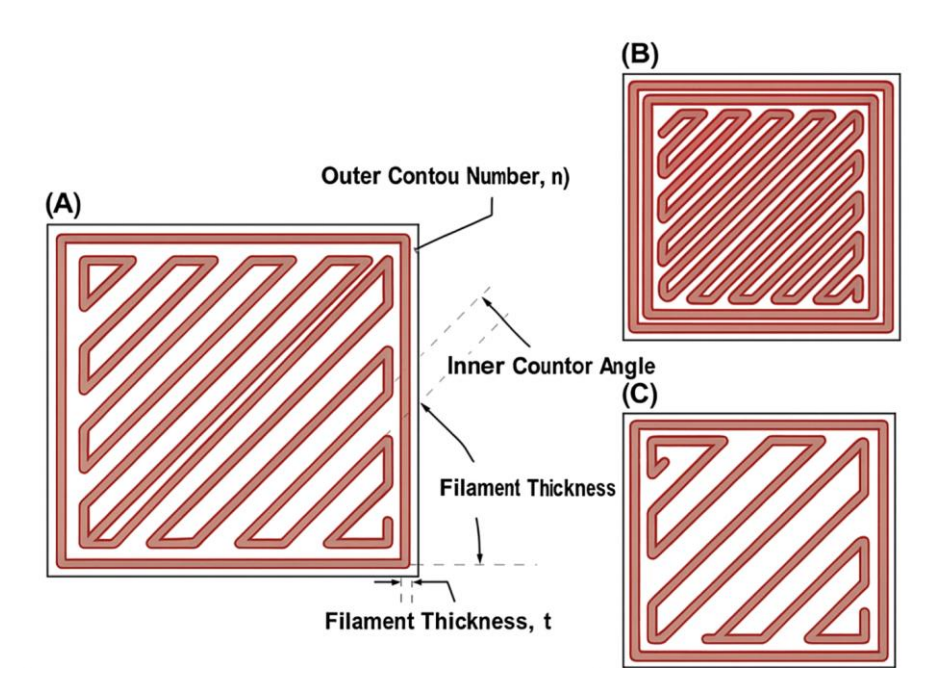


Figure 2.4 A) Toolpath variables, B) Toolpath variables, C) Sparse toolpath.

Improper selection of process parameters based on the material can result in several defects, including uneven layer deposition, weak adhesion between layers, rough surface finish, internal voids, and as a consequence, parts with reduced structural integrity [30].

A key consequence of the layer-by-layer fabrication process in FDM systems is that the printed parts exhibit anisotropic properties—meaning their mechanical strength and behavior vary with direction [24]. Because of this directional dependence, the part's placement and orientation on the build platform must be carefully determined according to the expected direction of mechanical stress during use [26, 27].

Figure 2.6 illustrates how different build orientations influence the mechanical behavior of printed parts.

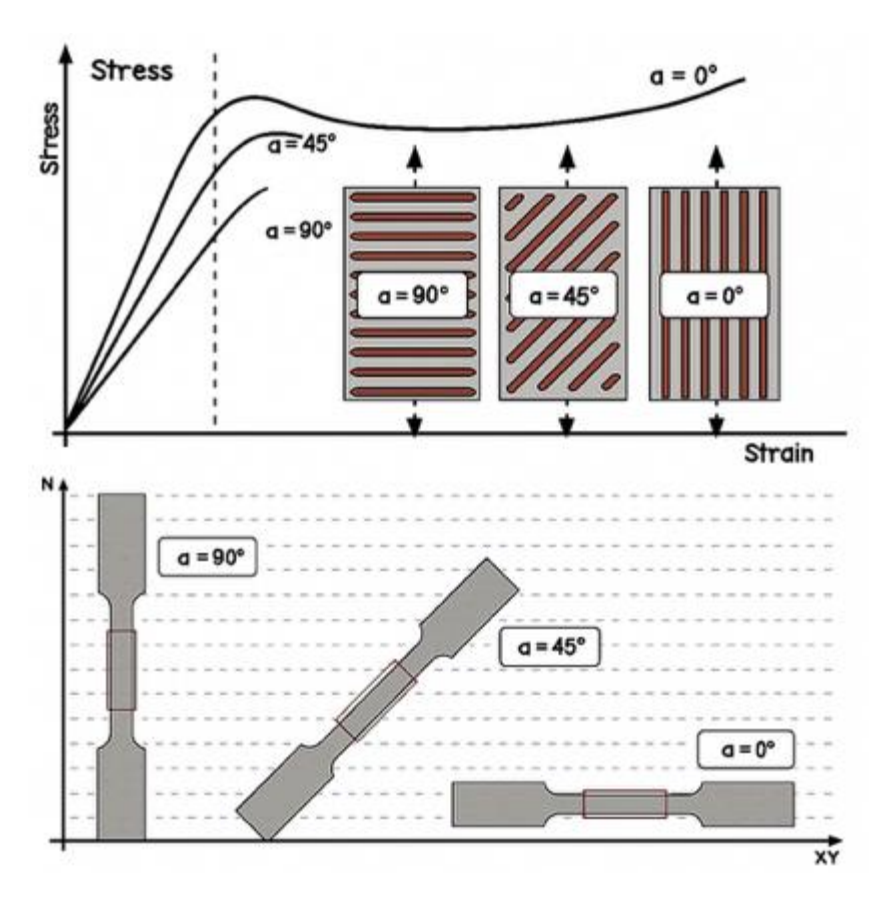


Figure 2.5 Influence of build orientation on the mechanical strength of the part. [29]

When the print layers are oriented in the same direction as the applied tensile force, the part generally shows improved strength and ductility along that axis. On the other hand, if the layers are oriented perpendicular to the load direction, the part tends to have the weakest mechanical performance. This weakness arises because the interlayer adhesion must bear the tensile load, and any defects or poor bonding between layers can act like notches, increasing stress concentration and promoting crack formation at lower loads. Parts printed at a 45-degree angle to the load direction usually exhibit intermediate tensile strength, falling between the parallel and perpendicular cases [27, 30].

In AM, part orientation will affect surface roughness greatly due to the build process layer by layer. Surface texture is an important factor in regard to both the appearance of the part and the mechanical performance of the part. In layered manufacturing, the part to be produced will exhibit the stair-step effect, to minimize the stair-step effect before printing, a detailed consideration in regard to the shape of the part should be considered based on its placement on the build platform. Figure 2.6 A demonstrates the impact of part placement on the resulting surface texture [29].

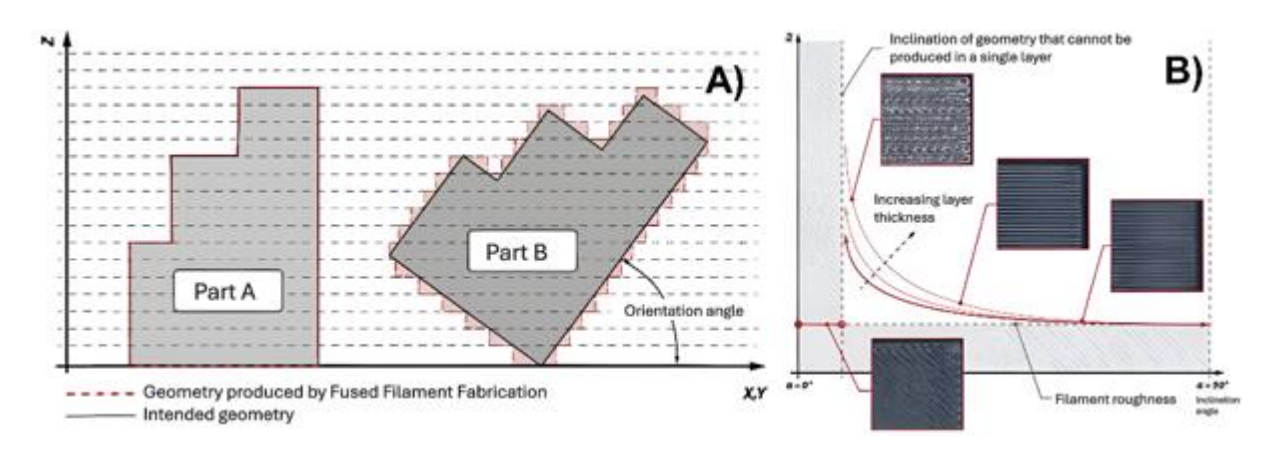


Figure 2.6 Presents the key factors influencing surface roughness, including (A) the orientation of the part and (B) the inclination angle along with the layer thickness.

For parts with angular geometries, positioning them parallel to the build platform tends to align naturally with their shape, resulting in minimal stair-stepping effects on the surface (as seen in Part A). In contrast, orienting the part at an angle introduces more pronounced layer stepping due to the nature of AM, which increases surface roughness (Part B). Surface roughness, typically measured as linear roughness (Ra), is strongly influenced by several factors: the part's inclination angle (α) relative to the platform, the layer thickness (Lt), and the surface orientation. When the upper surfaces of the part are aligned parallel to the platform ($\alpha = 0^{\circ}$), stair-step formation is minimized, leading to improved surface quality. Figure 2.6 B illustrates the relationship between the part's build angle and surface roughness. As shown, surface roughness is lowest when the angle α is 0° or 90°. Deviations from these angles, along with increased layer thickness, result in rougher surfaces. For this reason, parts should be oriented on the build platform in a way that optimizes surface finish, based on the intended function and visual requirements of the final product [27, 30].

Surface roughness is often unavoidable in components with certain geometries, leading to the desire to improve the surface finish. To improve the surface finish, many different techniques can be employed depending on the surface finish spec, including mechanical techniques such as sanding, polishing, filling, priming, painting, and varnishing. Beyond mechanical techniques, chemical techniques—such as an acetone bath or being exposed to chemical vapor—can be utilized to smooth and finish the surfaces of polymer components. In addition to enhancing the aesthetics of the part, thus producing realistic prototypes of designs, these finishing methods can improve resistance to the environment and thereby improve product durability and lifespan [31, 32].

2.2.2. Fused Granular Fabrication (FGF)

Fused Granular Fabrication (FGF) is a recent method in extrusion-based AM where polymer granules or pellets are directly fed into a heated screw extruder and deposited layer by layer to create a three-dimensional object [38]. This process does not require filament preparation, which is traditionally tedious, involving both a high-energy

consumption and high-cost aspect to the process, while allowing for industrial-grade and recycled materials to be used directly. As such, FGF represents an attractive approach to develop large-scale AM in a more sustainable manner, achieving much higher deposition rates and lower material costs than traditional Fused Filament Fabrication [39].

In the FGF process, polymer pellets are melted and transported through the nozzle by a screw-driven extruder, which deposits the material onto a heated build platform [40]. The extrusion rate and melt viscosity are regulated by the screw speed, barrel temperature, and feed rate, allowing for the processing of a broader suite of thermoplastics, including engineering-grade materials with high fill loadings. This versatility makes FGF a technology suited for applications requesting performance and mechanical strength, high throughput, or feedstock generated from post-industrial or recycled materials [41].

However, FGF faces certain limitations which affect its dimensional accuracy and mechanical homogeneity compared to filament-based printing. An increased nozzle diameter, higher flow rate, and less precise thermal regulation leads to uneven surfaces, porosity, and heterogeneous layer-to-layer adhesion [42]. In addition, the increased cooling rates experienced in open-chamber systems can lead to thermal gradients, producing warpage and shrinkage. While these issues may not be critical with most thermoplastics, they are especially problematic to semi-crystalline polymers like polypropylene (PP) or polyamide (PA) [42]. Addressing these issues generally requires closed build chambers, refined temperature profiles, and/or modified formulations potentially to improve bonding and reduce residual stresses between layers [40,42]. While these limitations exist, studies have demonstrated that FGF can produce polymer components with thermal or mechanical properties comparable to injection-molded parts when processing amorphous or low-shrinkage materials [39,41]. The ability to directly utilize industrial pellets, combined with its costeffectiveness and compatibility of recycled materials, make FGF a relevant method for large-scale sustainable AM [40,38].

2.2.3. Printing Process

The three main stages of AM for a 3D object are design, printing, and post-processing. The 3D printing production process starts off with a 3D model, created using computer-aided design (CAD) software or 3D scanned from a physical object, then converted to the standard triangulation language (STL) file format and then sliced into 2D images (layers) using slicing software [15,16].

The STL format only defines the surface of the 3D model as a network of triangles of varying sizes based on the required resolution. Shown is Figure 2.8.

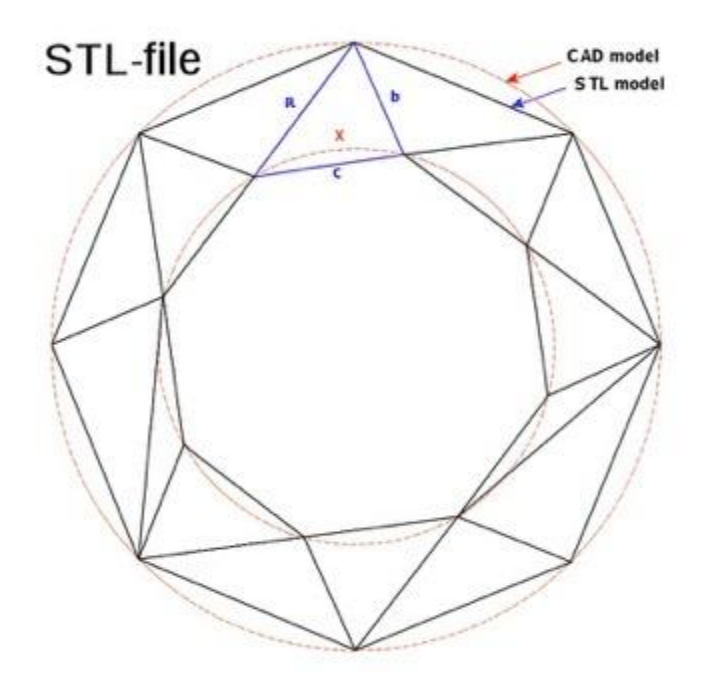


Figure 2.7 For the manufacturing process, the CAD-based model was exported to the Standard Triangulation Language (STL) format.

A 3D printed object is built layer by layer, and each layer must always rest on either the platform, the previous layer, or additional support. After creating the correct and most optimal orientation, the STL model is sliced into layers with a plane leaning on the platform surface (i.e., the xy plane). Each layer is built in the z direction and then repeated per layer contribution until the entire part is complete, as shown in Figure 2.8. [15]

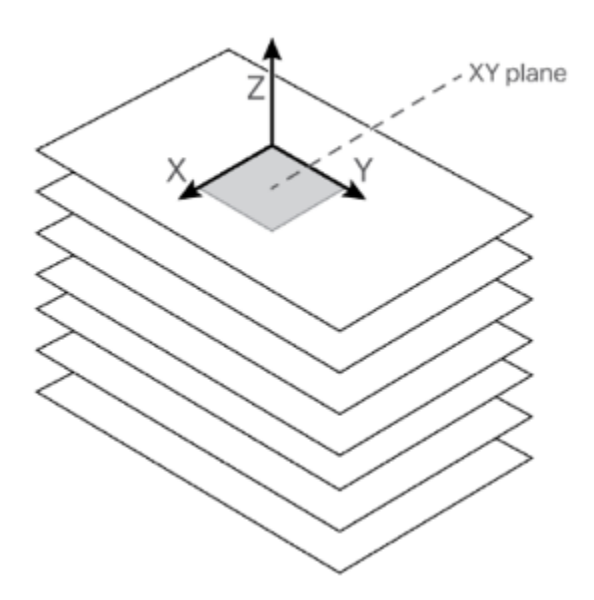


Figure 2.8 Fabrication through a layer-by-layer printing process.

The layer thickness is influenced by the specifications of the printer, the employed AM method, and the quality expectations desired. After the model has undergone slicing, the model is sent to the printer to be fabricated [15]. AM differs from traditional subtractive manufacturing techniques, where material is removed from the workpiece, and allows more efficient utilization of materials and reduced waste [15].

In the printing process, layers employed consecutively until the final geometry is presented on the build platform as a consolidated stack of printed layers. This asprinted object will be referred to as the 'green body', which indicates the object has unreacted monomers and can be cured by post-irradiation or post- thermal methods of curing [16], [33].

Post-processing is the final step involved in AM in order to achieve the intended 3D-printed part [16].

Removal of the support structures, in most cases, the optimization of the printing orientation will suffice to not require supports; however, when support structures are needed, they will be removed[16].

3. EXPERIMENTAL WORK

The purpose of this chapter is to present detailed information regarding the materials that were utilized during the study. The commercial names for the materials used are Bayblend T85 X RE, InnoEnd P1 M M112 BK, and Eplon+ 6 IMP BK Q2A505 along with the parameters for 3D printing and specific characterization techniques.

3.1. Materials

3.1.1. Bayblend T85 X RE

Bayblend T85 X RE is an engineering-grade thermoplastic from Covestro made from PC/ABS blends. The "RE" designation is for a grade that is partly assigned through mass balance according to the ISCC PLUS standard. Bayblend T85 X RE is designed principally for injection molding and has resistance to aging in humid environments, low volatile organic compound (VOC) emissions, and good odor properties. Bayblend® T85 X RE is suitable for use in applications requiring surface treatment, or painting; enhancing the applicability of Bayblend T85 X RE where aesthetics and environmental performance are necessary features. [34,35].

Bayblend T85 X RE has a well-balanced combination of stiffness and toughness. Its tensile modulus is 2,300 MPa and yield stress is 56 MPa. The nominal strain at break is over 50%, while the yield strain is around 4.9%. The notched Izod impact strength is 57 kJ/m² at 23 °C and 46 kJ/m² (-30 °C). Notched Charpy impact strength is 60 kJ/m² at 23 °C and 47 kJ/m² (-30 °C). This data show that the mechanical performance of the material is only slightly affected by temperature [34,35].

Depending on the load and heating rate, the Vicat softening temperature is 129–131 °C, and the heat deflection temperature is 127 °C at 0.45 MPa, and 106 °C at 1.80 MPa. The coefficient of linear thermal expansion (CLTE) is approximately 0.7 ×10⁻⁴/K between 23 °C and 55 °C, with similar values measured for both parallel and normal directions. These properties indicate reliable behavior relative to dimensional stability and deformation under thermal loading [34,35].

The melt volume-flow rate (MVR) is between 13-23 cm³/10 min at 260 °C with 5 kg load. The suggested melt temperature is 270-290 °C and mold temperature should be 70-90 °C. The molding shrinkage is between 0.55-0.75 % [34,35]. The mechanical, thermal, and impact properties of Bayblend T85 X RE are summarized in Table 3.1.

Property	Value	Standard / Test Method
Tensile Modulus (MPa)	2,300	ISO 5271/2
Yield Stress (MPa)	56	ISO 5271/2

Property	Value	Standard / Test Method
Yield Strain (%)	4.9	ISO 5271/2
Nominal Strain at Break (%)	> 50	ISO 5271/2
Notched Izod Impact Strength @ 23 °C (kJ/m²)	57	ISO 180/A
Notched Izod Impact Strength @ −30 °C (kJ/m²)	46	ISO 180/A
Notched Charpy Impact Strength @ 23 °C (kJ/m²)	60	ISO 179/1eA
Notched Charpy Impact Strength @ −30 °C (kJ/m²)	47	ISO 179/1eA
Vicat Softening Temperature (VST/B50) (°C)	129	ISO 306, 50 N; 50 °C/h
Vicat Softening Temperature (VST/B120) (°C)	131	ISO 306, 50 N; 120 °C/h
Heat Deflection Temperature (HDT/A, 1.80 MPa) (°C)	106	ISO 75-1/-2
Heat Deflection Temperature (HDT/B, 0.45 MPa) (°C)	127	ISO 75-1/-2
Coefficient of Linear Thermal Expansion (23–55 °C parallel/normal) (1/K)	' 0.7 ×10	⁴ ISO 11359-1/-2
Melt Volume-Flow Rate (MVR) (cm³/10 min)	13–23	ISO 1133, 260 °C / 5 kg
Recommended Melt Temperature (°C)	270– 290	Covestro datasheet
Recommended Mold Temperature (°C)	70–90	Covestro datasheet
Molding Shrinkage (parallel / normal) (%)	0.55– 0.75	ISO 294-4

Table 3.1 The mechanical, thermal, and impact properties of Bayblend T85 X RE.

3.1.2.Eplon+ 6 IMP BK Q2A505

EPLON+ 6 IMP BK Q2A505 refers to a specific grade of polyamide 6 obtained from high-quality post-industrial recyclables. It has been modified to improve impact performance, heat stabilization, and lubrication to make it particularly suited to injection molding applications. In terms of physical properties, the material exhibits a density of

1.10 g/cm³ at 23 °C which can be expected of a typical polyamide 6, while still providing molded dimensional accuracy. Dimensional stability is defined by a mold shrinkage of 1.6% in the parallel direction and 1.9% in the normal direction for a sample size of 2 mm. These results suggest that it will meet tight tolerancing in precision applications.

The mechanical properties indicate a strong engineered profile. The tensile modulus is 2,500 MPa dry, 1,900 MPa conditioned. The tensile strength is 45 MPa dry, 35 MPa conditioned and elongation at break is over 35% and over 50% respectively. The flexural properties show a modulus 2,100 MPa dry, 1,700 MPa conditioned with flexural strength measured at 85 MPa (dry) and 75 MPa (conditioned). The impact resistance is notable: notched Izod and Charpy impact resistance ranged from 20-30 kJ/m² depending on the conditioning. Unnotched samples showed "no break" at test conditions highlighting the tough nature of the material. The mechanical, thermal, and impact properties of EPLON+ 6 IMP BK Q2A505 are summarized in Table 3.2.

Property	Value	Standard / Test Method
Tensile Modulus (23 °C)	2,500 MPa (dry) / 1,900 MPa (cond.)	
Tensile Strength (23 °C)	45 MPa (dry) / 35 MPa (cond.)	ISO 527-2
Elongation at Break (23 °C)	>35 % (dry) / >50 % (cond.)	
Flexural Modulus (23 °C)	2,100 MPa (dry) / 1,700 MPa (cond.)	
Flexural Strength (23 °C)	85 MPa (dry) / 75 MPa (cond.)	
Notched Charpy Impact Strength (23 °C)	(cond.)	ISO 179/1eA
Unnotched Charpy Impact Strength (23 °C)		ISO 179/1eU
Notched Izod Impact Strength (23 °C)	(cond.)	ISO 180/1A
Unnotched Izod Impact Strength (23 °C)	No break	ISO 180/1U
Melting Temperature	220 °C	ISO 11357/1-3

Property	Value	Standard / Test Method
Flammability (0.8 mm)	НВ	UL 94 / EN 60695- 11-10
Density (23 °C)	1.10 g/cm³	ISO 1183
Injection Molding (parallel / normal)	Shrinkage 1.6 % / 1.9 %	ISO 294-4

Table 3.2 The mechanical, thermal, and impact properties of EPLON+ 6 IMP BK Q2A505.

3.1.3.InnoEnd P1 M M112 BK

The polymer called InnoEnd P1 M M112 BK is a recycled PP copolymer that has been commercially engineered for injection molding. It contains 12% mineral filler and stabilizers that improve its dimensional stability as well as mechanical balance and processing reliability. Considering also its physical properties, the compound has a density of 0.97 g/cm³ at 22 °C, which is normal for polypropylene-based formulations. The moisture content was less than 0.2% at test conditions and the ash content was 12%, an indication of the mineral filler volume. The melt flow index was 19 g/10 min (at 230 °C and 2.16 kg load), and indicates there is a good degree of flowability, helping show that the compound is suitable for injection molding.

The mechanical characteristics of InnoEnd P1 M M112 BK indicate a balance of strength and stiffness. The tensile strength is indicated to be 18 MPa with a tensile modulus of 1350 MPa and an elongation at break of less than 50%. The flexural is 18 MPa and a flexural modulus of 1700 MPa, thus confirming the reinforcing feature from the use of a mineral filler. The impact resistance is presented by notched Izod impact strength of 17 kJ/m² and notched Charpy impact strength of 14kJ/m². The unnotched samples, for both Izod and Charpy, did not break during testing, indicating sufficient toughness under less severe stress conditions. The mechanical, thermal, and impact properties of InnoEnd P1 M M112 BK are summarized in Table 3.3.

Property	Value	Standard / Test Method
Density (22 °C)	0.97 g/cm ³	ISO 1183-1
Moisture Content (130 °C, 15 min)	<0.2 %	ISO 15512
Ash Content (800 °C, 15 min)	12 %	ISO 3451-1

Property	Value	Standard / Test Method
Melt Flow Index (230 °C / 2.16 kg)	19 g/10 min	ISO 1133-1
Tensile Strength (22 °C, 50 mm/min)	18 MPa	ISO 527-2
Tensile Modulus (Elastic Modulus)	1350 MPa	ISO 527-2
Elongation at Break	<50 %	ISO 527-2
Flexural Strength (22 °C, 2 mm/min)	18 MPa	ISO 178
Flexural Modulus (22 °C, 2 mm/min)	1700 MPa	ISO 178
Notched Izod Impact Strength (22 °C)	17 kJ/m²	ISO 180
Unnotched Izod Impact Strength (22 °C)	No break	ISO 180
Notched Charpy Impact Strength (22 °C)	14 kJ/m²	ISO 179
Unnotched Charpy Impact Strength (22°C)	No break	ISO 179
Heat Deflection Temperature (1.8 MPa)	68 °C	ISO 75
Vicat Softening Temperature (50 N)	75 °C	ISO 306
Pre-Drying Temperature / Time	60–80 °C / 2–4 I	n Datasheet
Injection Molding Temperature	170–240 °C	Datasheet
Injection Pressure	80–120 bar	Datasheet

Table 3.3 The mechanical, thermal, and impact properties of InnoEnd P1 M M112 BK.

3.2. Printing Machine and Process Parameters

Tumaker NX 300 Modular is a medium-sized AM system that utilizes a modular architecture that enables different extrusion technologies to be used. It has a build volume of $300 \times 300 \times 250$ mm and closed print chamber for process stability (Figure 3.1) [36].

NX 300 Modular features an interchangeable extrusion head system. The printer can be configured in various ways: single or dual filament heads, single or dual pellet heads, and mixed filament–pellet configurations. This modularity allows Fused Filament Fabrication (FFF) and Fused Granular Fabrication (FGF) to be used on the same platform [36].

In this study, the FGF configuration of the Tumaker NX 300 Modular was employed. The printer was used with pellet feedstock as the material input.

The system can achieve nozzle temperatures as high as 300 °C and bed temperatures of 100 °C. The suggested feedstock size for pellet extrusion is recommended to be circular pellets of 3–5 mm in diameter. The machine achieves layer resolutions of 10 μ m. The approximate noise emissions when the system is operating with the enclosure closed are quoted as 44 dB, and under ideal conditions it is closer to 40 dB [36].



Figure 3.1 Tumaker NX 300 Modular

The Tumaker NX 300 Modular was operated using the slicing software Simplify3D. Simplify3D is a commercial software package that converts 3D digital models to AM, preparing them for 3D printing with G-code optimized for the material and printer in use. It provides manipulation options of advanced slicer parameters such as layer thickness, speed, or temperature.

3.2.1. Preparing The Materials and Process Parameters

As an initial step, Bayblend T85 X RE, InnoEnd P1 M M112 BK, and Eplon+ 6 IMP BK Q2A505 pellets underwent pre-drying to prepare them for 3D printing. Each material

was pre-dried under identical conditions of time and temperature. The pre-drying parameters are presented in Table 3.4.

Material	Pre-Drying Temperature (°C) Duration (h)
Bayblend T85 X RE	80	24
InnoEnd P1 M M112 BK	80	24
Eplon+ 6 IMP BK Q2A505	80	24

Table 3.4 The pre-drying parameters of the materials.

As the second step, the preparation of the digital models for printing was carried out. The dog-bone tensile specimens were designed according to the ISO 527-2 Type 5A standard and subsequently processed in the slicing software Simplify3D, which is used in conjunction with the Tumaker NX 300 Modular. In this stage, the geometrical models were converted into G-code, incorporating the printing parameters required for the FGF process with pellet feedstock.

In addition, the G-codes for the specimens used in the Dynamic Mechanical Analysis (DMA) and flexural tests were generated. These geometries were prepared in Simplify3D according to the ISO 6721 standard for DMA and the ISO 178 standard for flexural testing. Along with the tensile specimens designed under ISO 527-2 Type 5A, these standards were consistently applied across all three materials - Bayblend T85 X RE, InnoEnd P1 M M112 BK, and Eplon+ 6 IMP BK Q2A505 - ensuring uniform specimen design and comparability in the subsequent 3D printing process.

The slicing parameters for the 3D-printing process were determined in Simplify3D to ensure that all specimens and materials were printed under the same parameters. These slicing parameters included temperature of the nozzle and bed, as well as layer height, print speed, infill density, and cooling capability. By standardizing the slicing parameters, the impact of the material type variables was isolated in the testing of mechanical properties. Table 3.5 summarizes the specific settings of the parameters for the 3D-printing process used for this study.

Category	Parameter	Value	Unit
General	Extruder Toolhead	Tool 1	-
General	Nozzle Diameter	0.80	mm
General	Extrusion Multiplier	1.00	-
General	Extrusion Width (Manual)	0.80	mm

Category	Parameter	Value	Unit
Ooze Control	Use Retraction	Enabled	-
Ooze Control	Retraction Distance	4.50	mm
Ooze Control	Extra Restart Distance	0.00	mm
Ooze Control	Retraction Vertical Lift	0.00	mm
Ooze Control	Retraction Speed	2700.0	mm/min
Layer Settings	Primary Extruder	Right Extrude	er -
Layer Settings	Layer Height	0.2000	mm
Layer Settings	Top Solid Layers	4	layers
Layer Settings	Bottom Solid Layers	4	layers
Layer Settings	Outline Perimeters	2	-
Layer Settings	First Layer Units	Absolute	-
Layer Settings	First Layer Height	0.3000	mm
Layer Settings	First Layer Width	0.40	mm
Layer Settings	First Layer Speed	900.0	mm/min
Skirt/Brim	Use Skirt/Brim	Enabled	-
Skirt/Brim	Skirt Extruder	Right Extrude	er -
Skirt/Brim	Skirt Layers	1	-
Skirt/Brim	Skirt Offset	3.00	mm
Skirt/Brim	Skirt Outlines	3	-
Sparse Internal Infill	Infill Extruder	Right Extruder -	
Sparse Internal Infill	Infill Pattern	Rectilinear	-
Sparse Internal Infill	Internal Pattern Rotation	0	deg
Sparse Internal Infill	Infill Percentage	100	%
Sparse Internal Infill	Infill Extrusion Width	100	%
Sparse Internal Infill	Combined Infill Layers	1	layers

Category	Parameter	Value	Unit
Sparse Internal Infill	Outline Overlap	15	%
Sparse Internal Infill	Minimum Infill Length	5.0	mm
Sparse Internal Infill	Dense Infill Layers	0	-
Sparse Internal Infill	Dense Infill Percentage	50	%
Solid Layers	External Infill Pattern	Rectilinear	-
Solid Layers	External Pattern Rotation	0	deg
Solid Layers	Solid Infill Threshold Area	25.0	mm²
Solid Layers	Solid Infill Extra Expansion	0.0	mm
Solid Layers	Top Layer Extra Expansion	1.00	mm
Solid Layers	Top Layer Extrusion Modifie	r 100	%
Print Speeds	Default Printing Speed	3600.0	mm/min
Print Speeds	Outer Perimeter Speed	60	%
Print Speeds	Inner Perimeter Speed	80	%
Print Speeds	Top Layer Speed	90	%
Print Speeds	Solid Infill Speed	90	%
Print Speeds	Sparse Support Speed	90	%
Print Speeds	Dense Support Speed	60	%
Print Speeds	XY Travel Speed	18000.0	mm/min
Print Speeds	Z Travel Speed	2400.0	mm/min
Time Estimation / Motion	n XY Acceleration	1000.0	mm/s²
Time Estimation / Motion Z Acceleration		15.0	mm/s²
Time Estimation / Motion	n Extruder Acceleration	8000.0	mm/s²
Time Estimation / Motion	n XY Jerk	600.0	mm/min
Time Estimation / Motion	n Z Jerk	60.0	mm/min
Time Estimation / Motion	n Extruder Jerk	6000.0	mm/min

Category	Parameter	Value	Unit
Time Estimation /	Motion Max Extruder Flow Rate	750.0	mm³/min

Table 3.5 Detailed slicer configuration for the right extruder toolhead.

All three materials were processed using the same set of configurations in Simplify3D, but the temperature and fan speeds are configuration-specific to the material and various distinct values were used for each configuration. The processing parameters for the nozzle temperature, pre-heating chamber temperature, and fan speed are included in Table 3.6.

Material	Nozzle (Hot-End) Temperature(°C)	Pre-Heating Chamber (°C)	Fan Speed (%)
Bayblend T85 X RE	280	250	0
InnoEnd P1 M M112 BK	240	210	0
Eplon+ 6 IMP BK Q2A505	250	220	0

Table 3.6 The material-specific printing parameters.

The materials created with the 3D printer are illustrated in Figures 3.2, 3.3, and 3.4. These figures illustrate the finished appearance and shape of the printed specimens as a visual reference in the later experimental studies.

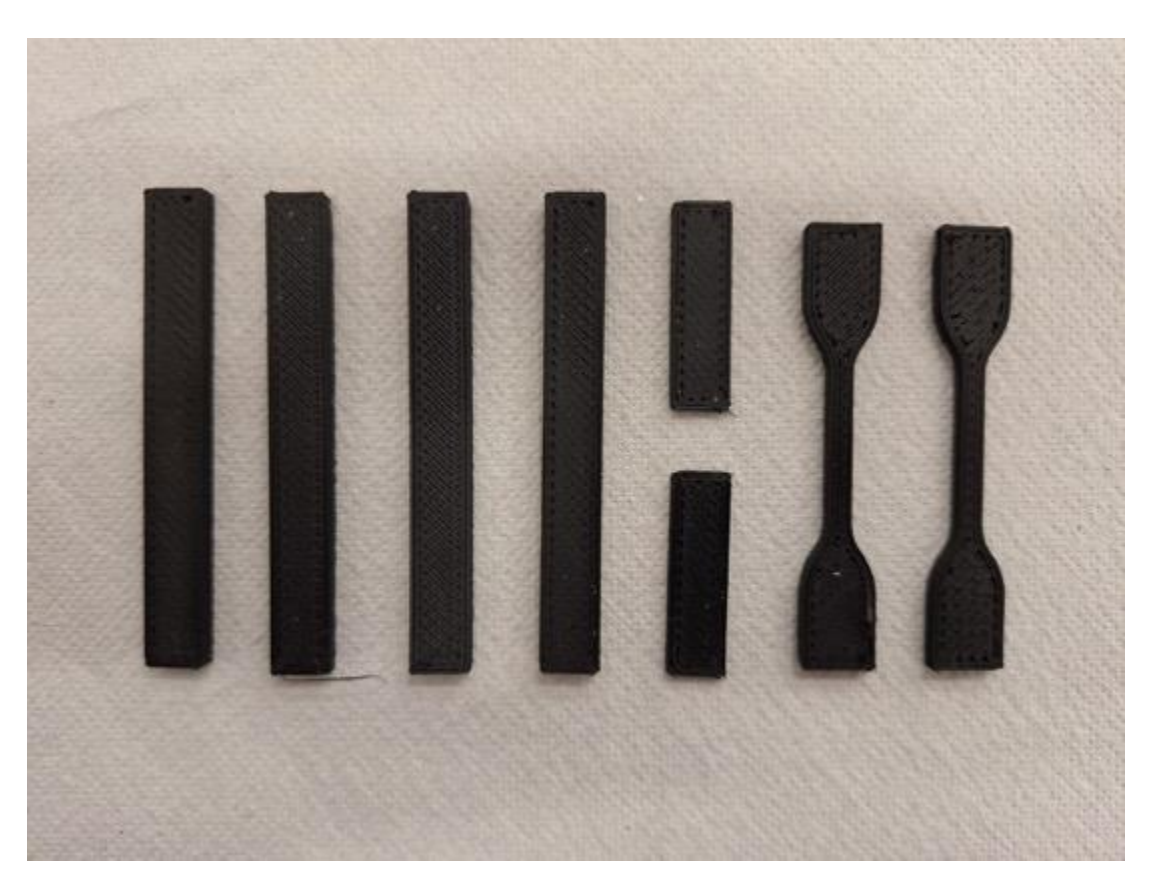


Figure 3.2 Printed specimens of Bayblend T85 X RE.

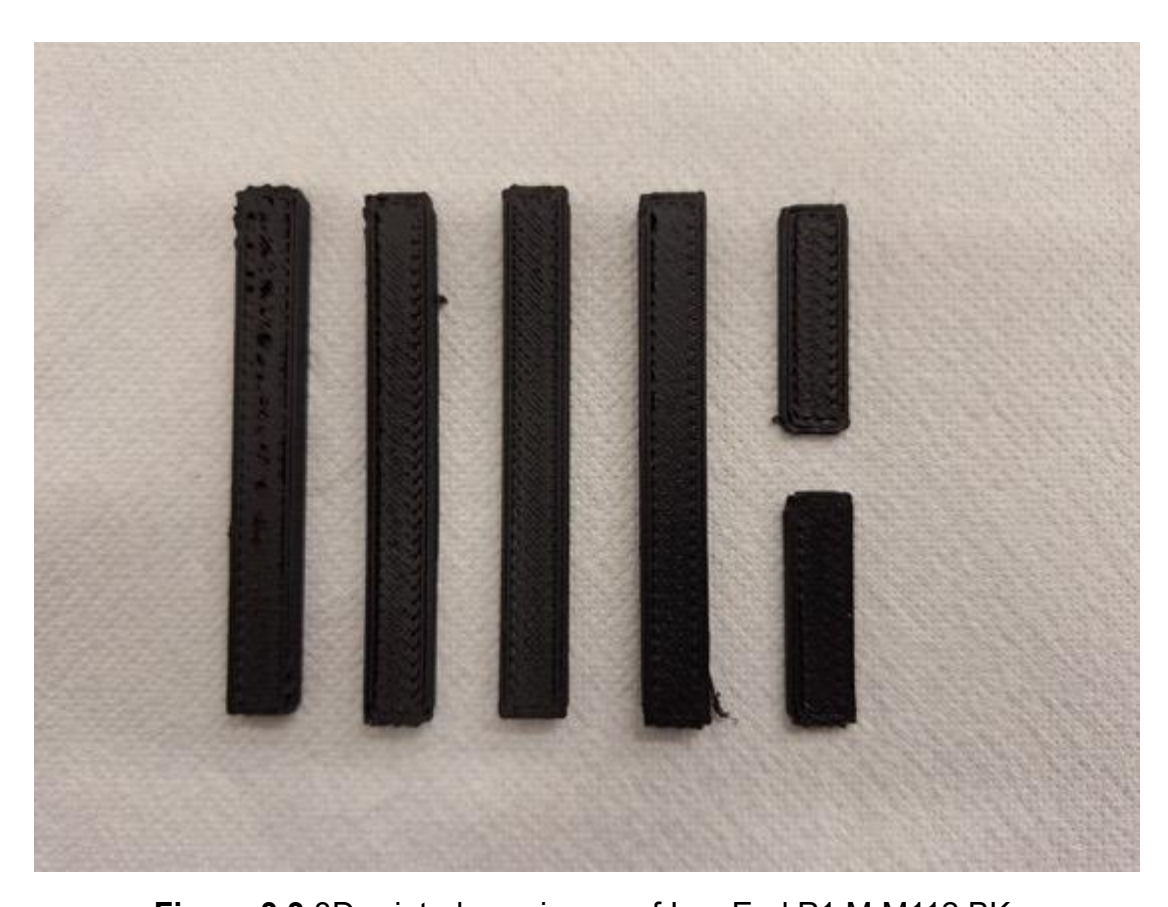


Figure 3.3 3D-printed specimens of InnoEnd P1 M M112 BK.

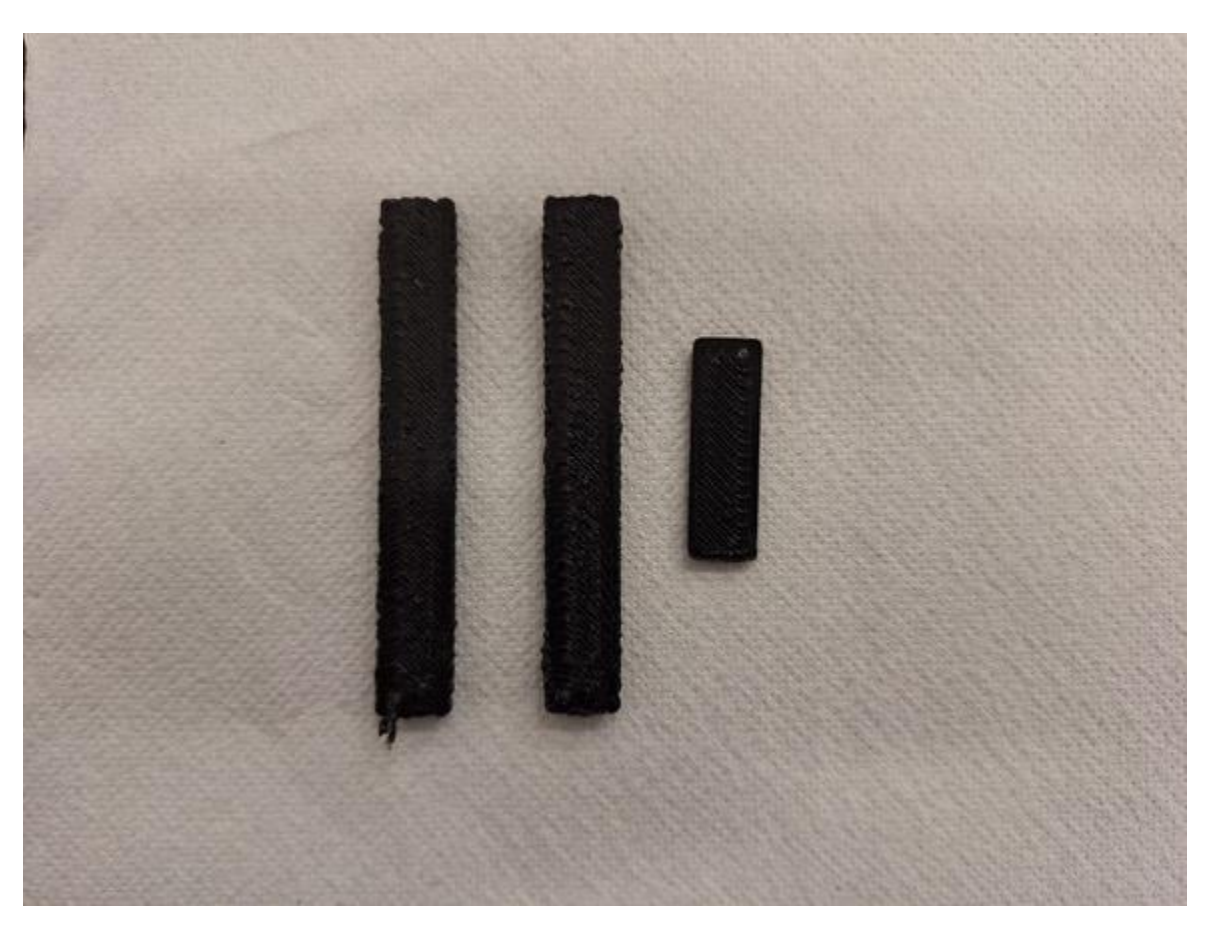


Figure 3.4 3D-printed specimens of Eplon+ 6 IMP BK Q2A505.

3.3. Characterization Methods

3.3.1. Differential Scanning Calorimetry

Differential Scanning Calorimetry (DSC) is a common analytical approach to investigating the thermal behaviour of materials. DSC identifies the heat flow into or out of a sample as a function of temperature or time while subjecting the sample to a controlled heating or cooling program. As part of the analysis, DSC requires the use of a reference material with known thermal properties commonly a metal like mercury or zinc. While changing the sample temperature according to a program, the temperatures of the reference and sample are measured, and the instrument then measures the heat from the temperature difference.

Differential scanning calorimetry is used to not only characterize the thermal properties of a material, it is also useful in determining the temperature at which a certain thermal phase transition takes place, including, but not limited to glass transition temperature, melting temperature (Tm), and crystallising exothermic events (Tc). Polymers are provided as example materials typically investigated using DSC, to determine the temperature of their thermal transitions (Tm, Tc and Tg) that largely govern the operation range over which a polymer is supposed to perform to a specification.

In this study, DSC was performed in order to determine the thermal properties of the pellets of all three materials, as well as their 3D printed forms. The interpretation of the

DSC data is based on the analysis of the thermograms produced from the experiment. A thermogram is a heat flow versus temperature, or time, plot. The thermogram analysis can provide information of the thermal transitions, as well as the thermal stability of the sample. Thermal transitions are a change in heat flow and can be seen as exothermic or endothermic peaks of the thermogram.

The Polyma DSC 214, manufactured by the Netzsch Group, was used for the tests performed in this study (Figure 3.5). The temperature ranges from -50 °C to 250 °C, and can be employed in the cooling phase as well as the heating phase. The heating and cooling rates are of 10 °C/min, two heating cycles and one cooling cycle were aimed for each of the samples. The instrument is supplied with a gas control transport system for the heating chamber; nitrogen transport was used at a flow rate of 50 mL/min.



Figure 3.5 Polyma DSC 214 System.

3.3.2. Thermogravimetric Analysis

Thermogravimetric analysis (TGA) is a method where a material's weight is measured as the temperature, or time, increases when the sample specimen is heated, under a controlled temperature program, within a controlled atmosphere. TGA was used to investigate the thermal stability of the cured materials [37]. In this study, TGA was performed on a Mettler Toledo TGA 851e (Figure 3.6). Temperatures were run from 25 °C to 800 °C at 10 °C/min heating rate, within oxide atmosphere. The thermal stability of the materials was determined from weight-loss versus heating curves.



Figure 3.6 Mettler Toledo TGA 851e System.

3.3.3. Dynamic Mechanical Analysis

Dynamic mechanical analysis (DMA) is a method for analyzing the viscoelastic properties of a polymeric material. The sample is subjected to a specific sinusoidal stress (or strain) to measure the time and temperature dependent deformation, or flow characteristics of the material. The storage modulus (E'), loss modulus (E") and the loss or damping factor (Tan δ) are the primary interesting output measures; E' measures the energy that is stored in the sample, and which will be released upon mechanical stress. E' is a measure of how elastic the material is, or how well it can store energy. Conversely, E" is a measure of how well the material can dissipate energy; E" describes the viscous component of the polymeric sample, equal to the loss of energy dissipated through friction and heat.

If the storage modulus is higher than the loss modulus, the material then can be described as being mainly elastic in nature. Conversely, if the loss modulus is higher than the storage modulus, the material has a viscous nature (it dissipates essentially more energy than it is able to store, like a fluid flowing).

The damping factor or loss factor, represented as Tan δ , is the ratio of the loss modulus to the storage modulus. Tan δ represents the energy dissipating, or damping, characteristic of the material. For instance, a material that has a Tan $\delta > 1$ will have more damping than a material with Tan $\delta < 1$, because Tan δ is > 1 means the loss modulus is greater than the storage modulus and thus the energy dissipating, viscous mechanisms will be more influential on the final material properties. DMA allows the ability to study the Tg of a polymer, which is an advantage over DSC, as maximum on the Tan δ curve as a function of temperature. The maximum peak of Tan δ is defined as the point of δ between the glassy and rubbery state.

DMA was performed using an Anton Paar MCR 702e Multi Drive (Graz, Austria) shown in Figure 3.7. And rectangular specimens (50 × 10 × 2 mm) prepared according to ISO 6721.



Figure 3.7 Anton Paar MCR 702e Multi Drive (Graz, Austria).

3.3.4. Tensile Test

Tensile testing applies a load to a specimen to assess the sample's response to uniaxial tension and develops a stress-strain curve which documents the response of the specimen. Tension testing examines a number of parameters, key parameters include break point, modulus of elasticity, yield strength and strain. ISO 527-2 is one of the most common testing standards when testing for tensile properties of a polymer product. Among the various parameters tested, tensile strength is the most often discussed parameter of the test and is taken at the highest force that the material can consistently withstand before failure or deformation and tensile modulus reflects material stiffness as a measured deformation under tensile load. This study includes tensile tests carried out per ISO 527-2 on specimens in the shape of an ISO 527-2-5A dog-bone shape using a universal testing machine. The tests were conducted using a crosshead speed of 1 mm/min to specimen failure and the tensile strength at break and tensile modulus was recorded.

In Figure 3.8 the instrument that was used to carry out the tensile tests. The Instron 6800 has 2 kN pneumatic grips and a load cell rated for 2 kN (<0.25% deviation). The

test has a 1 mm/min rate of deformation and a 50 mm grip separation. The displacement transducer is used to calculate deformation.



Figure 3.8 Instron 6800 System.

4. RESULTS AND DISCUSSION

In this study, thermal analyses and thermo-mechanical tests were conducted on Bayblend T85 X RE, InnoEnd P1 M M112 BK, and Eplon+ 6 IMP BK Q2A505. However, only Bayblend could be subjected to tensile testing. As shown in Figure 3.3 and 3.4, the other materials could not be printed into the desired optimal geometry using 3D printing. During the printing process, detachment and warping were generally observed, and closer inspection revealed defects within the layers. Consequently, these materials were excluded from further mechanical testing. Although the flexural test specimens fabricated from Bayblend appeared promising, they exhibited limping during testing, and the resulting data were too noisy to yield reliable results.

4.1. Characterization of Materials and Specimens

Thermal (DSC and TGA) and thermo-mechanical (DMA) analyses were performed on both the pellet and 3D-printed forms of Bayblend T85 X RE, InnoEnd P1 M M112 BK, and Eplon+ 6 IMP BK Q2A505, while Bayblend T85 X RE was additionally subjected to tensile testing. In the DSC thermograms, the red curve displays the first heating, which displays the thermal history of the material. The purple curve shows the second heating, directly capturing the thermal transitions without any previous effects. The green curve represents the cooling cycle, showing the crystallization or the relaxation response for cooling.

4.1.1. Differential Scanning Calorimetry

4.1.1.1. DSC of Bayblend T85 X RE in Pellet Form

In the following charts, it can observe the thermal transition through the changes in the heat flow measured. DSC of Bayblend T85 X RE in Pellet Form

An examination of the DSC curves for 1.2-TR, 1.4-TR, and 1.5-TR demonstrated no identifiable thermal transitions in the form of a glass transition (Tg), crystallization (Tc) or melting (Tm) event. The heat flow signals appear continuous and linear in character, while endothermic/exothermic peaks were not observed to any discernable degree which is evidence that the sample Bayblend T85 X RE obtained in pellet form was largely amorphous in Figure 4.1.

Similarly, there was no clear baseline shift corresponding to a glass transition so this again serves to affirm that there are disordered polymer chain distributions without molecular rearrangement in a specific temperature range. The amorphous discovery in pellet form could be attributed to quick cooling while compounding or through deliberate ways of partial amorphization during processing.

The DSC data of Bayblend T85 X RE in pellet form suggested a primarily amorphous structure and not crystalline phase. The amorphous structure could provide beneficial aspects such as impact resistance and optical clarity, while giving up thermal materials performance over a relatively wide use temperature range.

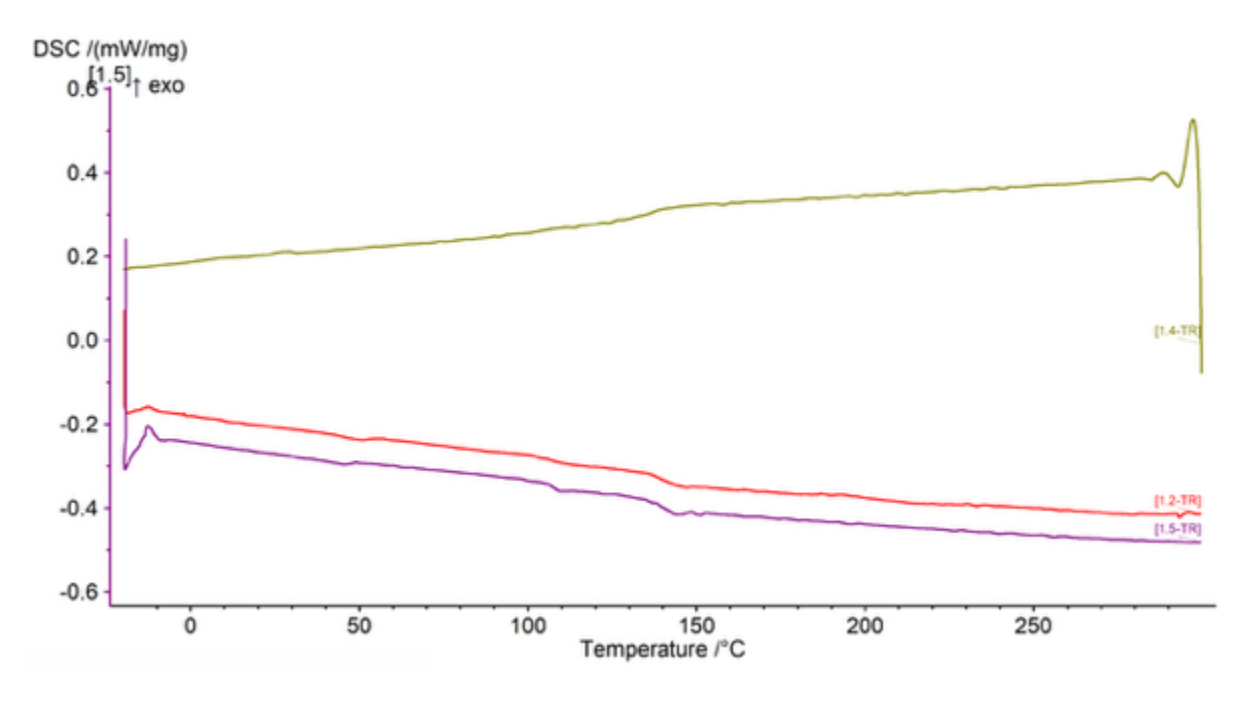


Figure 4.1 Differential Scanning Calorimetry (DSC) curves of Bayblend T85 X RE Pellets.

4.1.1.2. DSC of 3D Sample of Bayblend T85 X RE

No distinct melting or crystallization peaks were observed, indicating that the sample remains largely amorphous. However, a subtle slope changes around 123 °C in the second heating scan (~1.5-TR) could correspond to the glass transition temperature (Tg). This temperature aligns well with the documented Vicat softening temperature of approximately 125 °C for Bayblend T85 X RE. The Tg appearing slightly below this range supports the amorphous structure and indicates preserved structural integrity after printing in Figure 4.2.

In the upper temperature range, we (between ~280–290 °C) did not see any clear melting or degradation peaks above background signals; the only signal noise we observed was likely instrument artifact. Overall, the material has demonstrated thermal stability after a 3D printing process.

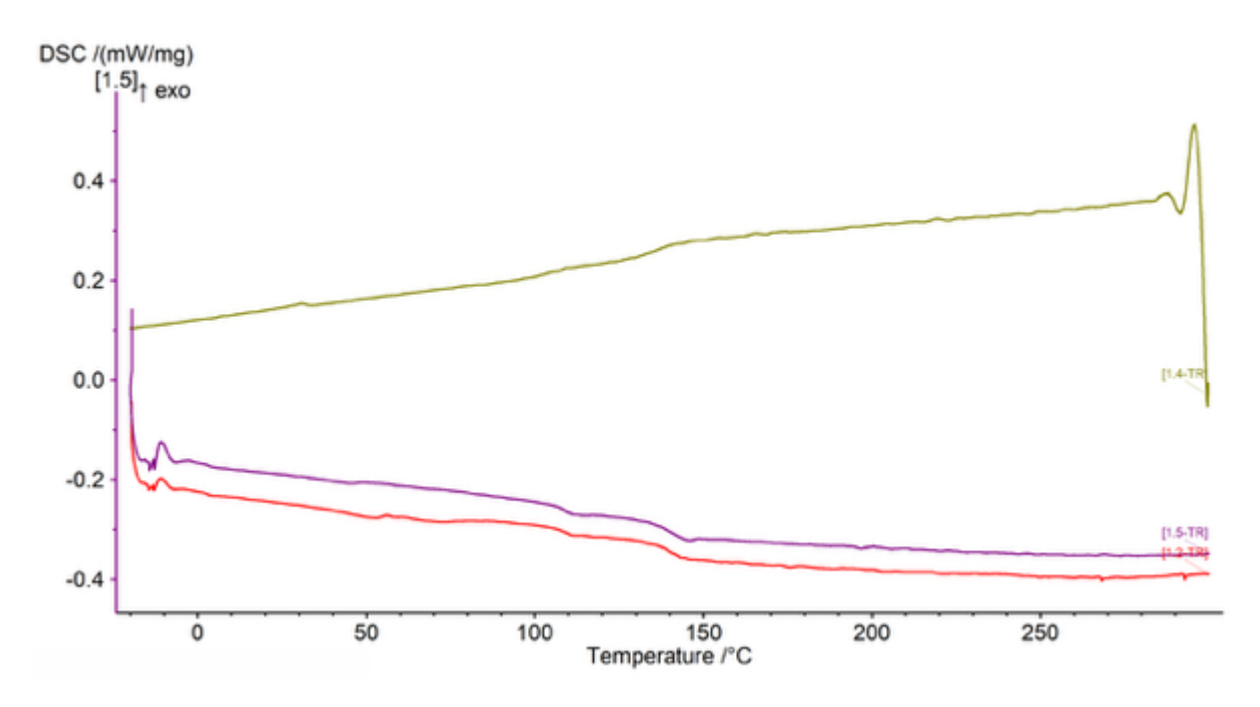


Figure 4.2 Differential Scanning Calorimetry (DSC) curves of 3D Sample of Bayblend T85 X RE.

4.1.1.3. DSC of InnoEnd P1 M M112 BK in Pellet Form

Figure 4.3 illustrates the DSC thermograms that clearly showed relevant thermal transitions, such as glass transition temperature (Tg), crystallization temperature (Tc), and melting temperature (Tm). Tg was roughly reported at 54.3 °C, corresponding to the threshold temperature of molecular mobility of the amorphous regions of polymer, which connects to the increased change in mechanical properties above this temperature. The relatively low Tg value indicates that the material properties would lose rigidity in the close temperature range of room temperature. In the cooling scan, there was a separate, exothermic peak at approximately 136 °C, which corresponds to the crystallization temperature. This peak is indicative of the reorganizing of polymer chains segment in the formation of crystalline lattices which is showing the material is semi-crystalline in nature. This enthalpy of crystallization was calculated to be at 65.25 J/g, demonstrating there is crystallinity being developed during the cool down phase at the given cooling rate.

The thermal analysis of the polymer revealed a melting enthalpy (ΔH_m) of 56.1 J/g confirming the development of crystallinity. To quantitatively determine the crystalline-to-amorphous ratio of the material, the degree of crystallinity (X_c) was calculated using the relationship in Equation 1:

$$X_c(\%) = \frac{\Delta H_m}{\Delta H_m^0} \times 100$$

Equation 1: Formula for Calculating the Degree of Crystallinity

where:

- ΔH_m : melting enthalpy of the sample measured by DSC (J/g).
- ΔH_m^0 : theoretical equilibrium melting enthalpy for 100% crystalline polymer (J/g).

For the calculation, the literature-established value for the equilibrium melting enthalpy of 100% crystalline PP, $\Delta H_m^0 \approx 207$ J/g, was used as the reference value.

$$X_c(\%) = \frac{56.1 J/g}{207 J/g} \times 100$$

$$X_c(\%) = 27.1\%$$

The calculated degree of crystallinity for the sample is 27.1 %.

There is a notable endothermic peak in the heating scan at roughly 170 °C, to correlate to the melting temperature of the crystalline domains. The melting enthalpy was calculated to be 65.3 J/g. The relatively low degree of crystallinity ($\approx 31.5\%$) indicates a dominant amorphous phase, which suggests the polymer possesses increased flexibility and toughness, consistent with its semi-crystalline nature. The high enthalpy of crystallization and melting shows good crystallization potential and thermal cycling resistance. Given the melting temperature, a processing window of approximately 190–210 °C is recommended, which would allow it to be processed using manufacturing processes such as injection molding or extrusion.

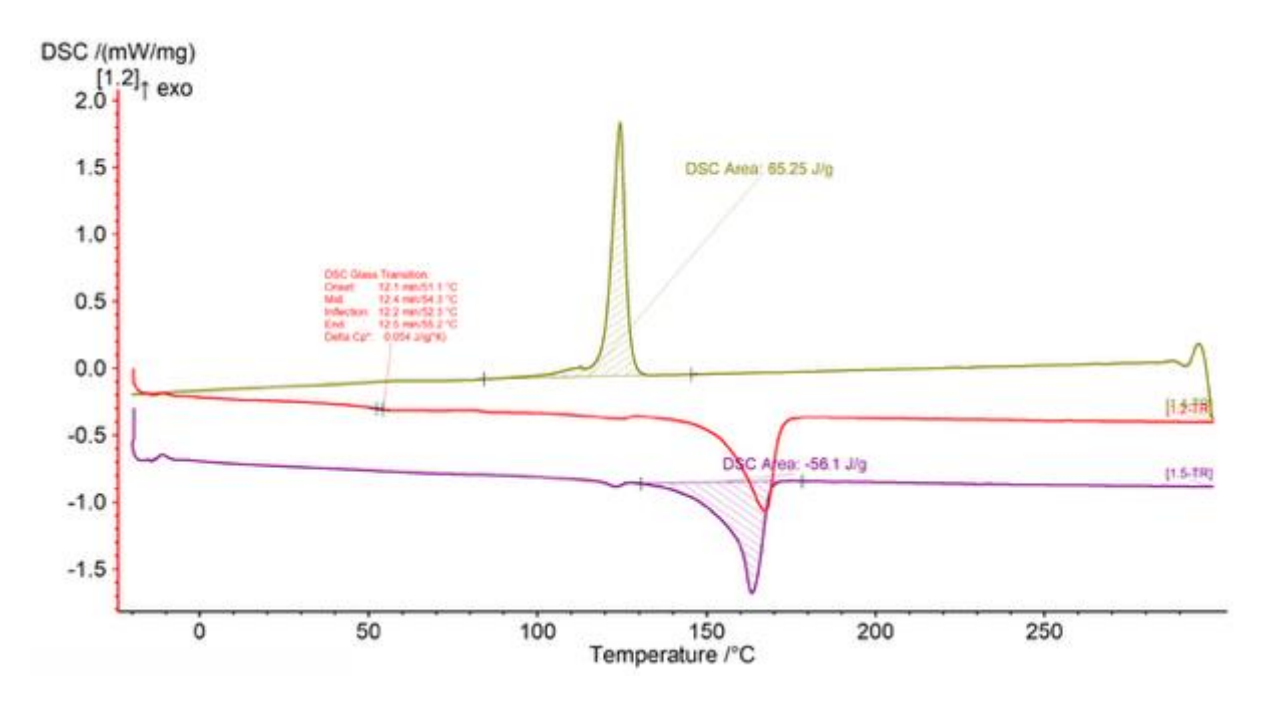


Figure 4.3 Differential Scanning Calorimetry (DSC) curves of InnoEnd P1 M M112 BK Pellets.

4.1.1.4. DSC of 3D printed specimen of InnoEnd P1 M M112 BK

Figure 4.4 shows that results from the initial heating scan revealed that the glass transition temperature (Tg) initiated at 38,3 °C, with the midpoint at 41,3 °C and conclusion at 43,3 °C. The associated change in heat capacity (Δ Cp) was calculated to be 0.091 J/(g·K). The low Δ Cp suggests that the morphology is primarily semicrystalline, which limits chain mobility probably due to rapid solidification and restricted movement resulting from the 3D process.A sharp endothermic peak located at about 170 °C corresponds to the polymer melting temperature Tm with an enthalpy of 68.27 J/g. An exothermic crystallization peak was observed during cooling at approximately 138 °C, with an enthalpy of crystallization -66.55 J/g indicating that the polymer chains do have some ability to reorganize into an ordered structure upon cooling.

The thermal analysis of the polymer revealed a melting enthalpy (ΔH_m) of 66.55 J/g upon heating, which is the primary evidence used to quantify the developed crystallinity. To quantitatively determine the crystalline-to-amorphous ratio of the material, the degree of crystallinity (X_c) was calculated using this value and the literature-based enthalpy for 100% crystalline PP (ΔH_m^0 = 207J/g) and found to be 32.1%. This calculated value confirms that the polymer exhibits a semi-crystalline morphology.

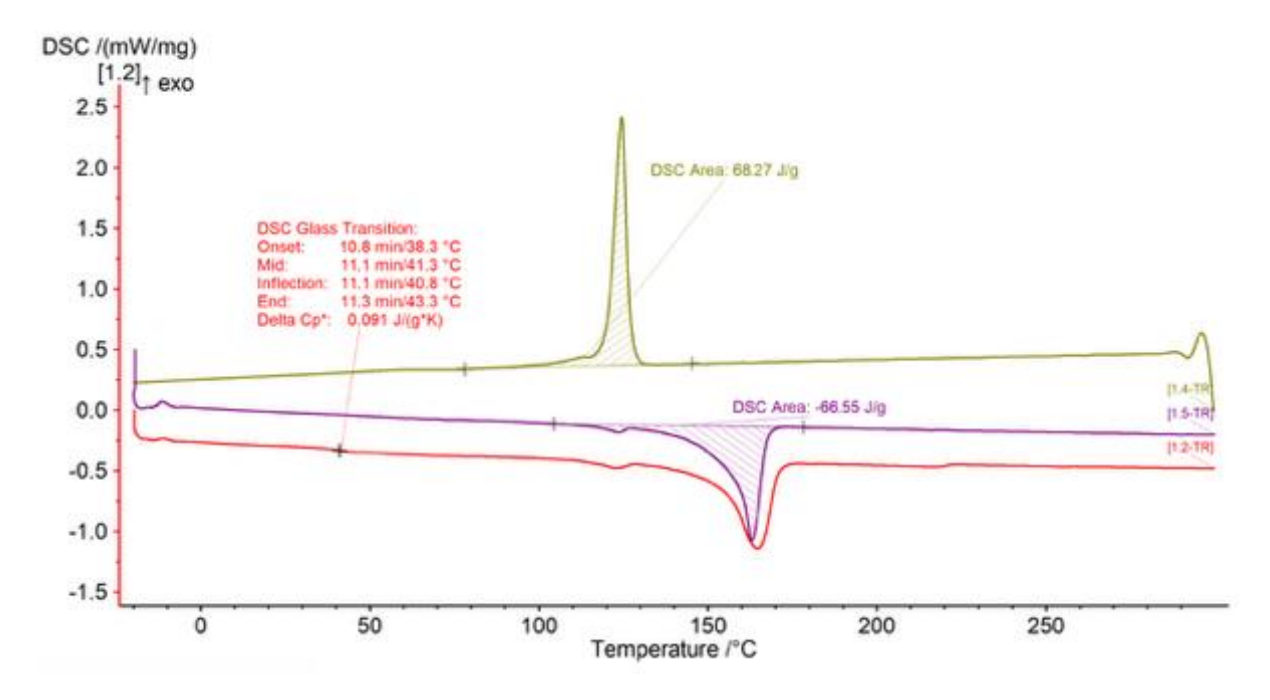


Figure 4.4 Differential Scanning Calorimetry (DSC) curves of 3D Sample of InnoEnd P1 M M112 BK.

4.1.1.5. DSC of Eplon+ 6 IMP BK Q2A505 in Pellet Form

In the second heating run (1.5-TR), the glass transition temperature (Tg) was established at a midpoint of 46,7 °C, where the onset, inflection, and end temperatures were 46,7 °C, 52,3 °C, and 59,4 °C, respectively. The respective change in specific heat capacity (Δ Cp) was calculated to be was 0.067 J/g·K. The analysis showed both

exothermic crystallization and endothermic melting transitions at elevated temperatures.

$$X_c(\%) = \frac{\Delta H_m}{\Delta H_m^0} \times 100$$

$$X_c(\%) = \frac{47.4 J/g}{190 J/g} \times 100$$

$$X_c(\%) = 25 \%$$

The degree of crystallinity (%Xc) of the PA6 sample was determined to be 25 %, calculated from the ratio of the measured melting enthalpy from the first heating scan (Δ Hm = 47.4 J/g) to the theoretical melting enthalpy of 100% crystalline PA6 (Δ H_100% = 190 J/g). This result, in conjunction with the clear observation of both a glass transition (Tg) and a melting endotherm (Tm) in the DSC thermogram, confirms that the material possesses a semi-crystalline structure composed of both amorphous and crystalline regions.

The absence of a cold crystallization peak in the first heating scan indicates that this crystalline structure was already established during its manufacturing process and was not subjected to rapid cooling. Furthermore, the crystallization enthalpy during the controlled cooling cycle (Δ Hc = 56.76 J/g) being higher than the melting enthalpy validates the material's potential to achieve a higher level of crystallinity under slower cooling conditions. The glass transition temperature of the Eplon+ 6 IMP BK Q2A505 Pellet was observed at 46.7 °C, which is relatively low. This indicates that polymer chains will become mobile at low temperatures.

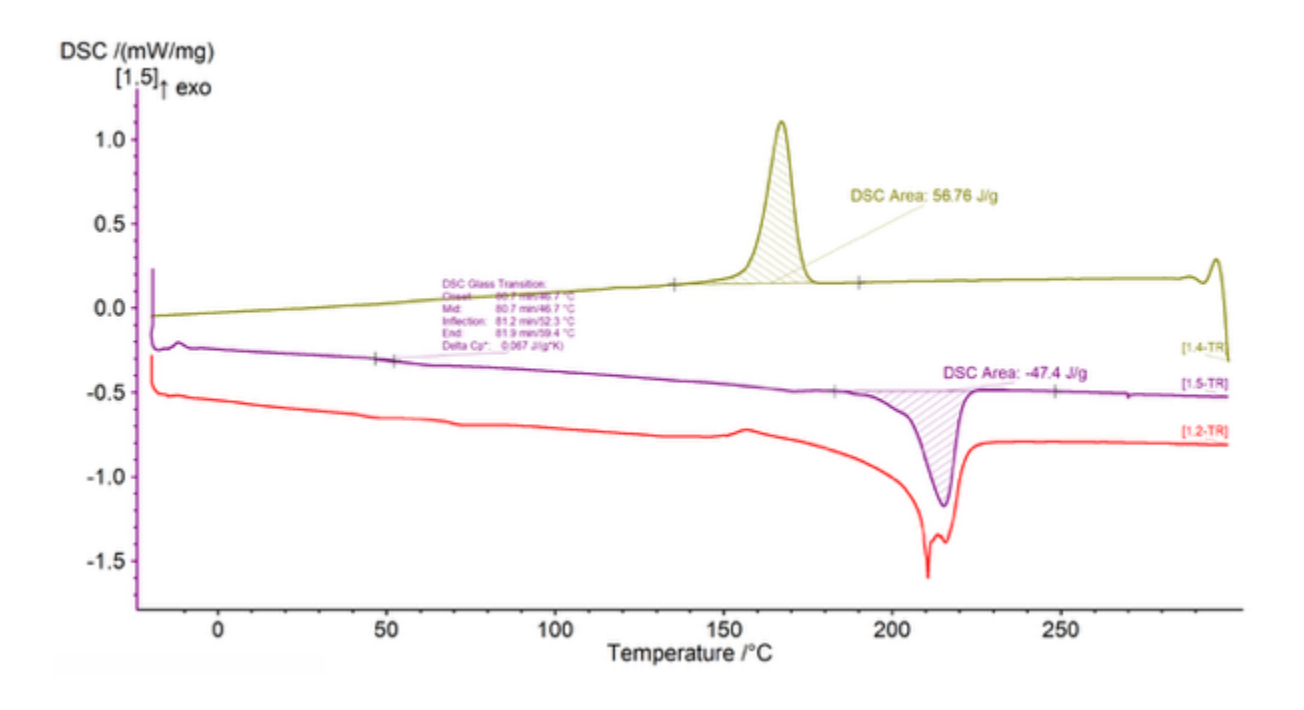


Figure 4.5 Differential Scanning Calorimetry (DSC) curves of Eplon+ 6 IMP BK Q2A505 Pellets.

4.1.2. Thermogravimetric Analysis

The stability of printed specimens was evaluated for thermal stability with TGA analysis.

4.1.2.1. TGA of Bayblend T85 X RE in Pellet Form

In Figure 4.6 TGA of the Bayblend T85 X RE in pellet form indicated that the material had mass stability up to around 350 °C, implying good thermal stability. The first decomposition stage began around 390 °C, and the maximum rate of mass depletion (thermal degradation) as measured by the first derivative (DTG), occurred at 412 °C. During this stage, the mass decreased from 100% to approximately 92%, with almost 8% weight loss. The major thermal degradation took place from approximately 420 °C to 520 °C with the greatest DTG peak occurring around 500 °C. Within this temperature range, the mass decreased from ~92% to ~35–40%, which is about 52–57% weight loss. The third, less significant thermal degradation event was noticed from around 540 °C to 560 °C, with the mass further decreasing from ~35–40% to ~5%. Upon reaching a temperature of 600 °C, the remaining mass was determined to be approximately 5% which demonstrates almost all degradation occurred with minor loss of inorganic mass. Characteristic degradation temperatures were found to be: $T \square \% \approx 405$ °C, $T \square \square \% \approx 485-490$ °C, and DTG peak of Tmax ≈ 500 °C.

Parameter	Symbol	Value (°C)
Temperature at 5% weight loss	T□%	≈ 405
Temperature at 50% weight loss	T□□%	485–490
Maximum degradation rate temperature (DTG		_
peak)	Tmax	≈ 500

Table 4.1 Thermal degradation parameters obtained from TGA analysis of Bayblend T85 X RE pellets.

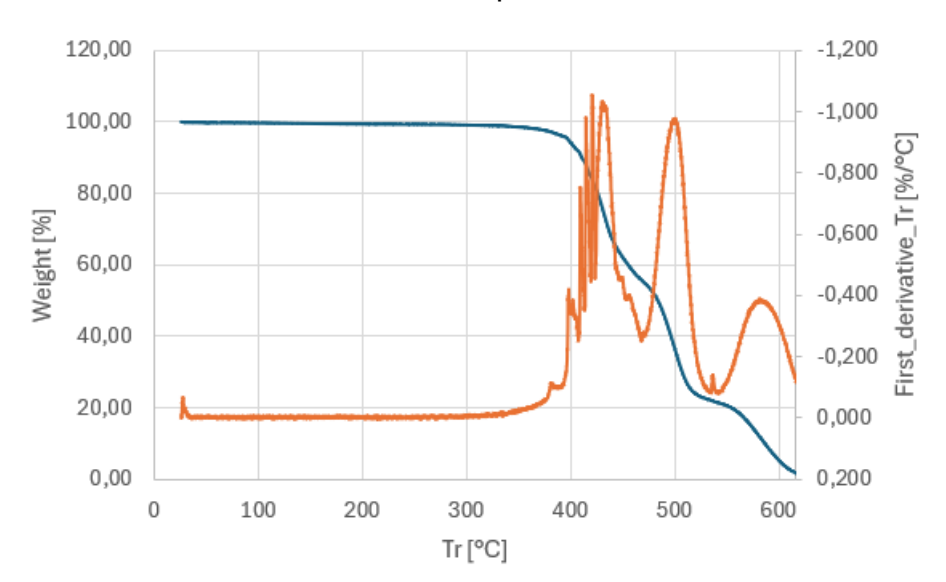


Figure 4.6 TGA/DTG curves of Bayblend T85 X RE pellets.

4.1.2.2. TGA of 3D printed specimen of Bayblend T85 X RE

TGA analysis of the Bayblend T85 X RE 3D sample showed that the material was stable to as high as about 350 °C in Figure 4.7. The first decomposition was indicated between 370–430 °C, with a peak rate of degradation at 420 °C in the DTG curve. During this thermal event, the mass decreased from 100% to approximately 84%, resulting in a loss of about 16% of its initial mass. A second major decomposition step occurred from 430-510 °C, with a clear DTG peak around 460-470 °C. In this temperature region, the mass decreased from ~84% to ~40%, accounting for an additional ~44% in weight loss. A third but less capable decomposition step occurred between 510–600 °C with a less pronounced peak in the DTG detected at ~540–550 °C. At this stage, the mass decreased from ~40% to ~6%. At the termination of TGA at 600 °C, the residual mass was ~6%. The characteristic decomposition temperatures revealed $T \square \% \approx 395$ °C, $T \square \square \% \approx 475$ °C, and $T \square X \approx 420-470$ °C.

Parameter	Symbol	Value (°C)
Temperature at 5% weight loss	T□%	≈ 395
Temperature at 50% weight loss	T□□%	≈ 475
Maximum degradation rate temperature (DTG		
peak)	Tmax	420–470

Table 4.2 Thermal degradation parameters obtained from TGA analysis of 3D sample Bayblend T85 X RE

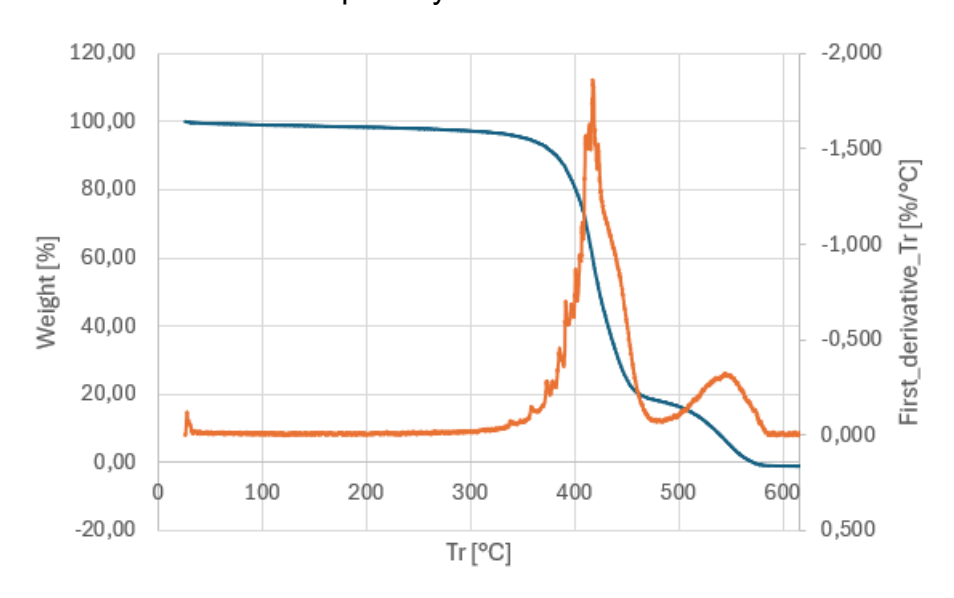


Figure 4.7 TGA/DTG curves of 3D sample Bayblend T85 X RE.

4.1.2.3. TGA of InnoEnd P1 M M112 BK in Pellet Form

In Figure 4.8 the TGA analysis of InnoEnd P1 M M112 BK in pellet indicated that the material was stable until approximately 300 °C. The primary stage of decomposition occurred from 310–400 °C, with the peak degradation rate occurring around 370 °C in the DTG curve. This stage saw a mass loss from 100% to approximately 12%, which corresponds to a weight change of about 88%. After 400 °C, no notable secondary decomposition was detected, and as the curve levels off, it signals that most of the degradation has occurred. At 600 °C, the residual mass was approximately 12%. The corresponding temperatures associated with decomposition were found to be $T \square \% \approx 320$ °C, $T \square \square \% \approx 360$ °C and $T \bowtie 370$ °C.

Parameter	Symbol	Value (°C)
Temperature at 5% weight loss	T□%	≈ 320
Temperature at 50% weight loss	T□□%	≈ 360
Maximum degradation rate temperature (DTG peak)	Tmax	≈ 370

Table 4.3 Thermal degradation parameters obtained from TGA analysis of InnoEnd P1 M M112 BK Pellets.

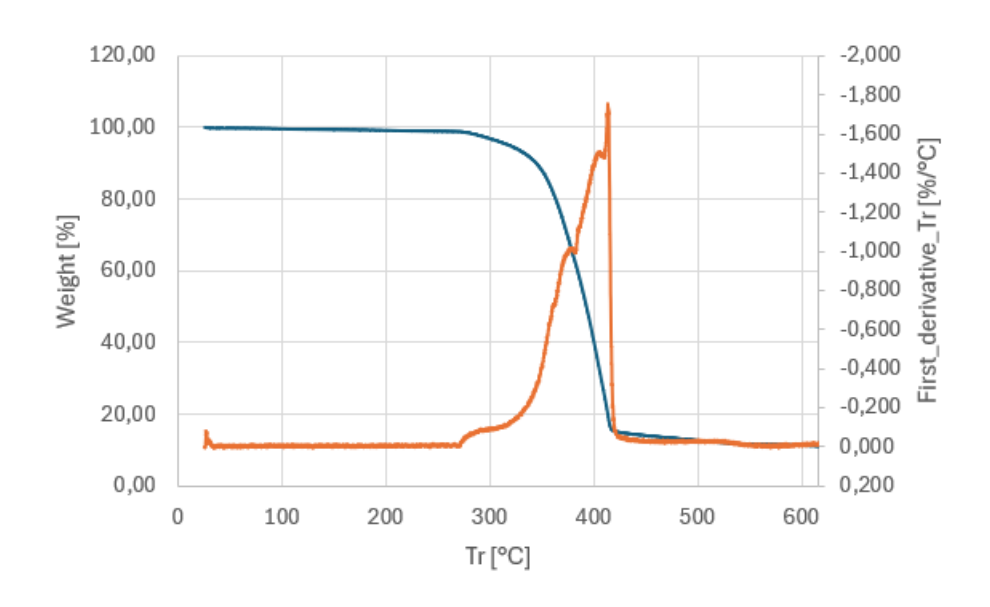


Figure 4.8 TGA/DTG curves of InnoEnd P1 M M112 BK Pellets.

4.1.2.4. TGA of 3D printed specimen of InnoEnd P1 M M112 BK

The TGA analysis of the Innoend 3D specimen suggested that it remained stable for the temperature limit of approximately 280–300 °C. Then the first major decomposition occurred in the range of 300–400 °C, exhibiting a peak degradation rate at around 370–380 °C in the DTG graph. In that stage, mass loss of the sample dropped from 100% to roughly 22%, corresponding to a weight loss of ~78%. There was no further significant weight loss above 400 °C level in the DTG curve, indicating degradation

was nearly complete. The residue mass was measured at ~22% at 600 °C. The characteristic values of the TGA analysis were T $_{-}$ % \approx 315 °C, T $_{-}$ 0% \approx 355–360 °C, and Tmax \approx 370-380 °C.

Parameter	Symbol	Value (°C)
Temperature at 5% weight loss	T□%	≈ 315
Temperature at 50% weight loss	T□□%	≈ 355 – 360
Maximum degradation rate temperature (DTG peak)	Tmax	≈ 370–380

Table 4.4 Thermal degradation parameters obtained from TGA analysis of 3D Sample of InnoEnd P1 M M112 BK.

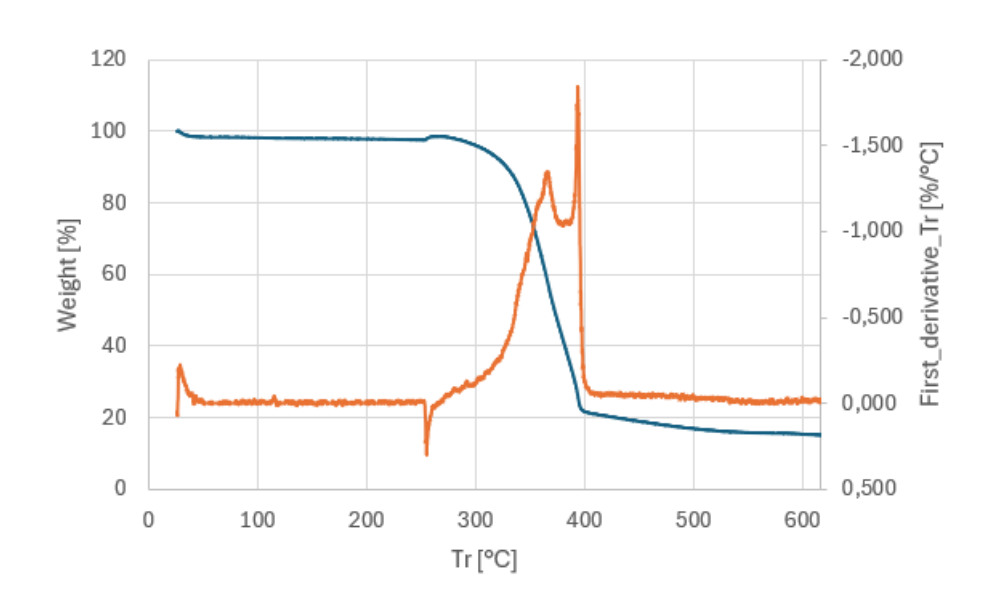


Figure 4.9 TGA/DTG curves of 3D Sample of InnoEnd P1 M M112 BK.

4.1.2.5. TGA of Eplon+ 6 IMP BK Q2A505 in Pellet Form

The TGA of the Eplon+ 6 IMP BK Q2A505 pellets indicated the material remained thermally stable to a temperature of approximately 350 °C in Figure 4.10. The primary decomposition stage took place between 380 °C and 470 °C, and the maximum rate of weight loss occurred at a temperature range of approximately 440 °C to 445 °C according to the derivative TGA (DTG) graph. During this primary decomposition stage, the sample weight decreased from 100% to approximately 20%, representing an approximate weight loss of 80%. From 470 °C, the rate of weight loss rapidly slowed down and a small degree of weight loss continued up to 600 °C. The final residual mass at the end of the measurement was approximately 8–10%. The decomposition temperature parameters were recorded as $T \square \% \approx 360$ °C, $T \square \square \% \approx 420$ °C and when rate of weight loss was at its maximum was recorded at Tmax ≈ 440 to 445 °C.

Parameter	Symbol	Value (°C)			
Temperature at 5% weight loss	at 5% weight loss T□%				
Temperature at 50% weight loss	T□□%	≈ 420			
Maximum degradation rate temperature (DTG peak)	Tmax	440–445			

Table 4.5 Thermal degradation parameters obtained from TGA analysis of Eplon+ 6 IMP BK Q2A505 in pellets.

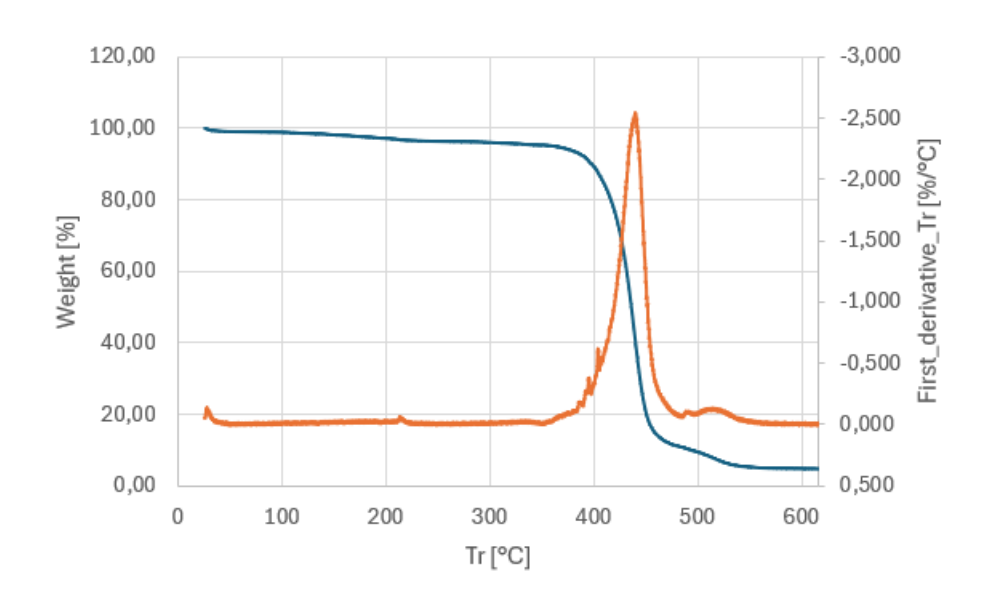


Figure 4.10 TGA/DTG curves of Eplon+ 6 IMP BK Q2A505 in pellets.

4.1.3. Dynamic Mechanical Analysis

To observe the viscoelastic behavior of three polymeric materials, Dynamic Mechanical Analysis (DMA) was carried out using Bayblend T85 X RE, InnoEnd P1 M M112 BK, and Eplon+ 6 IMP BK Q2A505 while varying the temperature.

The plot of storage modulus (E') compared to temperature in Figure 4.11 shows the change in material rigidity (stiffness) as we increase the temperature. At low temperatures, around -30°C, the InnoEnd P1 M M112 BK has the highest storage modulus of approximately 4560 MPa; the Eplon+ 6 IMP BK Q2A505 value is approximately 3560 MPa. All three material's modulus significantly decrease as the temperature increases, showing they have crossed their glass transition regions. The Eplon+ material's fixed drop in modulus occurs at around 0°C, while InnoEnd waits until around 30°C before any significant drop in modulus. The Bayblend T85 X RE material, at the start of this investigation, around 30°C, has a modulus of approximately 1160 MPa, and has a great retention of that value up to around 110°C, indicating a plateau region for the material. The Bayblend material has two drops in modulus, each around 110-140°C. In comparison at 100°C, the Bayblend material has the most rigidity

as represented by its modulus of approximately 890 MPa, compared to the InnoEnd material at approximately 367 MPa, and Eplon+ is at approximately 207 MPa.

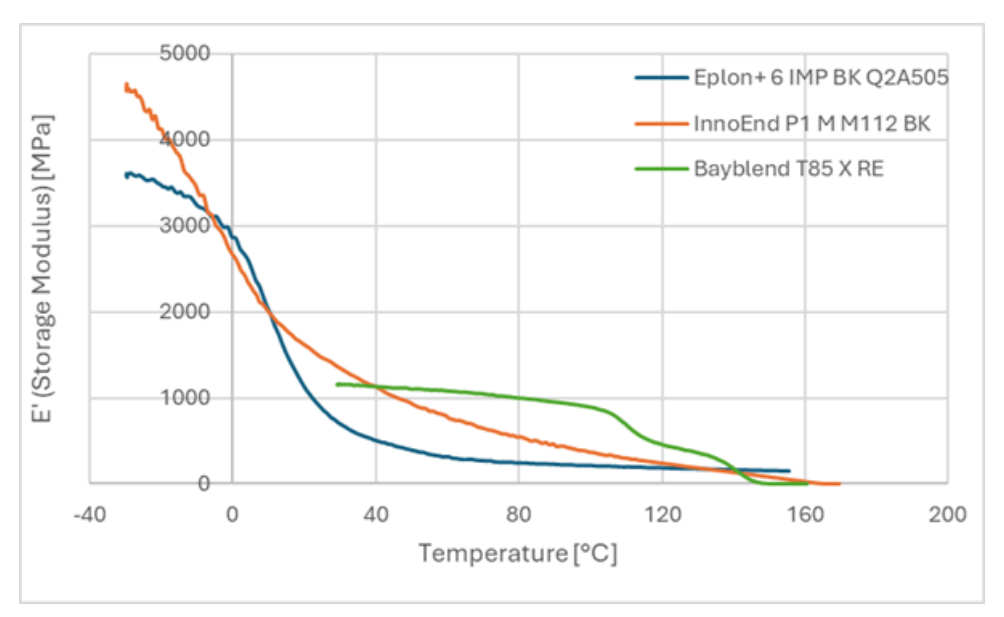


Figure 4.11 Storage modulus (E') as a function of temperature for Bayblend T85 X RE, InnoEnd P1 M M112 BK, and Eplon+ 6 IMP BK Q2A505 samples.

The loss modulus (E") plots in Figure 4.12 shows that the three materials being compared are fundamentally different in how they dissipate energy and in having different (molecular) relaxation processes. Both polymers, Eplon+ 6 IMP BK Q2A505 and InnoEnd P1 M M112 BK, also demonstrate nearly identical behavior, featuring their primary relaxation peaks well below the temperature range of interest. The plots for these two materials present merely the decreasing slope of their low-temperature primary peaks and a loss modulus that decreases continuously with increasing temperature, beginning with a loss modulus above 380 MPa at -30°C for the Eplon+ material and nearly 520 MPa for the InnoEnd. The Bayblend T85 X RE material not only distinguishes itself completely by presenting two distinct and defined relaxation peaks but also has the first broad peak and second defined relaxation peak within the temperature range of interest. The first peak presents a maximum value of 100 MPa at around 110°C and the second peak presents a maximum value of 75 MPa at around the 140°C mark. Bayblend is consequently identified as a thermally much more stable material that has low energy dissipation at low temperature but has both of two different molecular relaxation mechanisms that are activated at high temperatures.

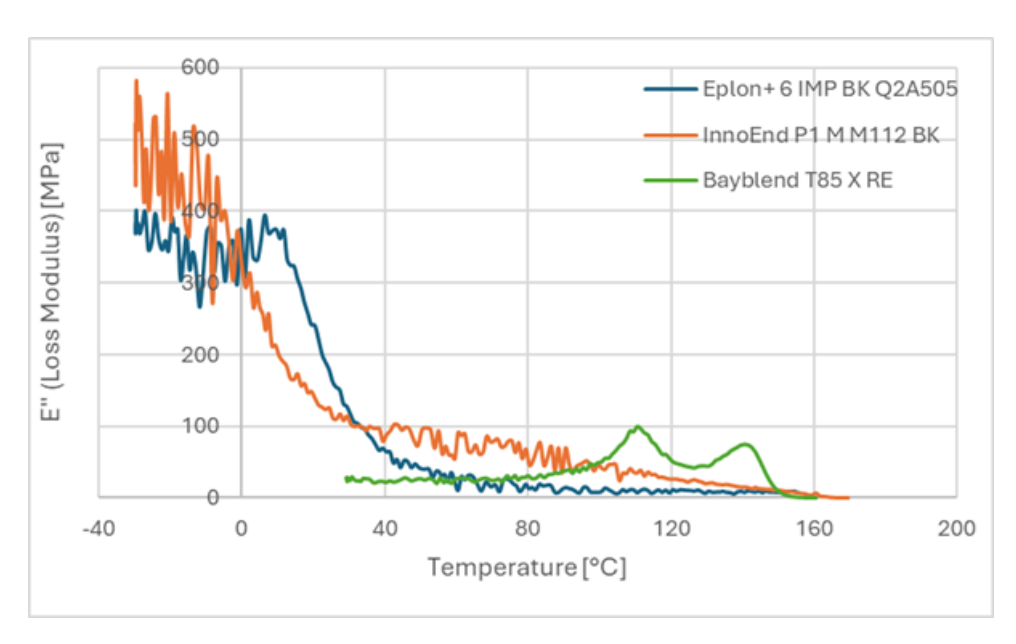


Figure 4.12 Loss modulus (E") as a function of temperature for Bayblend T85 X RE, InnoEnd P1 M M112 BK, and Eplon+ 6 IMP BK Q2A505 samples.

The analysis of the Tan δ curves in Figure 4.13 clearly shows the qualitative differences of the materials' damping behavior. Eplon+ 6 IMP BK Q2A505 has a clear and broad peak located at around 25° C and has a peak value of approximately 0.2; this is the traditional damping response due to the glass transition for the material (Tg). In stark comparison, the InnoEnd P1 M M112 BK material does not show a significant damping peak in the temperature range studied, retaining very low Tan δ values (below ~0.1). This suggests that InnoEnd has either a very weak glass transition or that Tg is outside of the test window, resulting in the material having little damping response. Bayblend T85 X RE is wholly different, as it shows a two-stage relaxation response. First, a low magnitude and broad peak of approximately 0.15 is observed at ~115° C, which is the Tg of one of the blend components. However, the curve is completely dominated by a second extremely sharp and high intensity peak at 150° C, well above 2.0. This peak is a clear indicator that the material is entering the terminal flow region, thereby losing its structural integrity and ceasing its solid-like behavior.

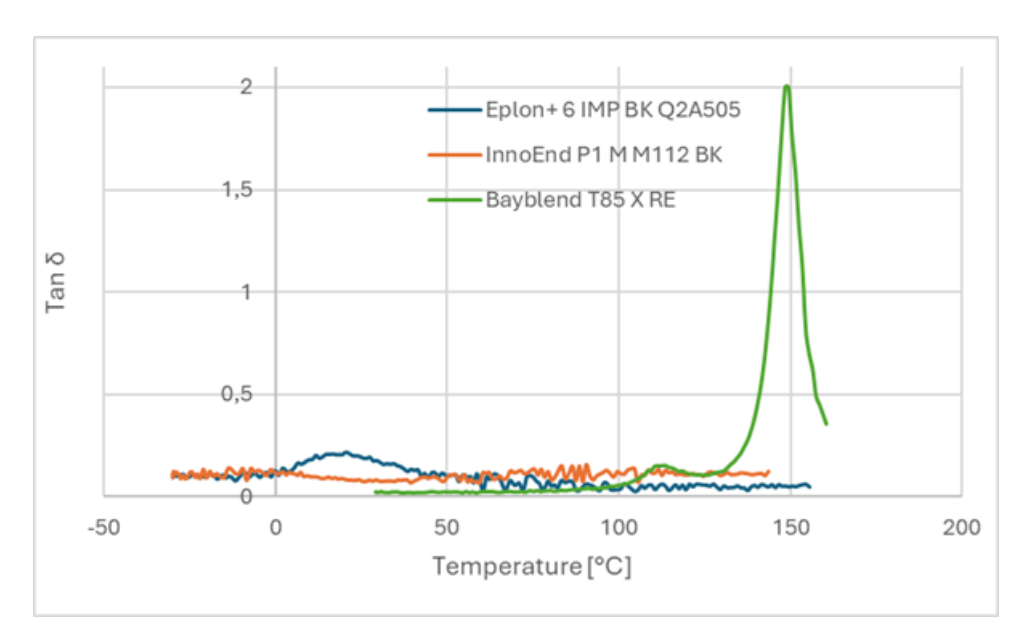


Figure 4.13 Tan δ as a function of temperature for Bayblend T85 X RE, InnoEnd P1 M M112 BK, and Eplon+ 6 IMP BK Q2A505 samples.

4.1.4. Tensile Test

Tensile tests were performed according to the ISO 527-2 Type 5A standard on 3D printed Bayblend T85 X RE specimens. There was a significant variation in mechanical performance for the four specimens, demonstrating that the 3D printing process parameters can significantly alter the structural integrity and mechanical behavior of the material.

The elastic modulus values of the specimens varied from 111 MPa to 291 MPa, illustrating noticeable differences in stiffness of the specimens. The highest modulus was reported for specimen 2 at 291 MPa, elevating the expectation of better interlayer adhesion and density of material internal to the sample. Specimen 3 exhibited the lowest modulus at 111 MPa, and may have had weak layer adhesion, or voids created during the 3D printing process. The notable differences reported in specimens exhibit the inherent anisotropy of additively manufactured polymers that are sensitive to variations in the print direction, infill pattern, and temperature.

The elongation at break data varied broadly from 7% to 98%. Specimen 1 rounded 98% elongation under tensile load, while specimen 3 showed a small amount of elongation with a relatively brittle failure. The fact there is a difference in the elongation at break values suggests that the level of molecular orientation and interlayer adhesion created during the printing process have an influence on ductility in 3D-printed parts. The significant opposite end data means an understanding of the specific mechanical behavior is not consistent for Bayblend T85 X RE under the print conditions.

For the tensile strength at break, the observed values were between 40 MPa to 47 MPa. When comparing the other parameters there was not as much variance in the tensile strength, which indicates that even if the printing quality differs, the material maintained its loading capability to a relative steady state. The highest value was the highest tensile strength was for specimen 4 (47 MPa), likely due to optimized process parameters used to increase layer-to-layer bonding.

The results show that 3D printing has a very noticeable impact on Bayblend T85 X RE's stiffness and ductility while the tensile strength remains relatively unchanged. These results highlight the significance of optimizing the process, primarily with regard to printing orientation, layer adhesion, and thermal management, for improved uniformity and reliability in the mechanical behavior of additively manufactured Bayblend

Property	Specime n 1	Specime n 2	Specime n 3	Specime n 4	Averag e	Standard Deviation
Elastic Modulus (MPa)	125	291	111	169	174	78
Elongation at Break (%)	98	70	7	33	52	39
Tensile Strength at Break (MPa)	40	45	41	47	43	3

Table 4.6 Mechanical Properties Obtained from Tensile Testing of 3D-Printed Bayblend T85 X RE

CONCLUSION

The primary objective of this study was to determine whether polymer parts produced by AM (3D printing) could achieve mechanical and thermal properties comparable to those obtained through conventional injection molding. Three recycled polymer systems - Bayblend T85 X RE (PC/ABS blend), Eplon+ 6 IMP BK Q2A505 (PA6), and InnoEnd P1 M M112 BK (PP) - were examined using a combination of thermal and mechanical characterization techniques, including Differential Scanning Calorimetry (DSC), Thermogravimetric Analysis (TGA), Dynamic Mechanical Analysis (DMA), and tensile testing. While all materials were successfully processed in injection-molded form, only Bayblend T85 X RE could be printed reliably using the Fused Granular Fabrication (FGF) process. The other two materials, PA6 and PP, exhibited significant detachment and warpage during printing, making mechanical testing of their printed forms infeasible.

The DSC measurements indicated notable differences in the reaction of the amorphous and semi-crystalline materials during the 3D printing process. In contrast to the poor thermal response results during the 3D printing of Bayblend T85 X RE being a source of concern, the pellet and the 3D-printed version were both found to be amorphous with no distinct melting or crystallization peaks observed. A slight glass transition near 123 °C was observed in the 3D printed version, consistent with the Vicat softening temperature obtained for the injection molded reference. This provides additional confirmation that the 3D printing method does not change the thermal transitions of the materials and does not promote crystallization. On the other hand, Eplon+ 6 (PA6) and InnoEnd (PP) exhibited unique melting and crystallization peaks indicative of semi-crystalline materials. The crystallinity of PA6 was around 25-30 % and of PP around 30 %. Although these levels of crystallinity increase mechanical strength of injection-molded parts, they also caused high internal stresses, shrinkage, and interlayer delamination in the printed specimens, thus, providing an explanation for warpage and detachment.

The TGA results further confirmed these observations. Bayblend had very good thermal stability, with little mass loss until above 430–450 °C for both the pellet and printed specimens. The degradation onset and mass loss were very similar to the injection-molded data, suggestive of no thermal degradation of the polymer from the FGF printing process. Both PA6 and PP had earlier degradation onsets (around 380 °C and 350 °C, respectively) as indicated by their lower oxidative stability as semi-crystalline materials. Nevertheless, all materials still had sufficient stability for thermal processing below 300 °C.

Dynamic Mechanical Analysis (DMA) offered information on the viscoelastic properties of the materials. For Bayblend T85 X RE polymer, the storage modulus (E') held fairly steady up to the glass transition temperature, then gradually declined, consistent with the behavior of an amorphous polymer. The damping factor (tan δ) peak near 125 °C matched well with the Tg derived from the DSC data, confirming stable viscoelastic transitions. The alignment between the analyses showed that the interlayer adhesive bonding within the 3D printed Bayblend was adequate to maintain an elastic response

similar to, or greater than, that of the injection molded material. On the other hand, for the semi-crystalline PA6 and PP samples, distinct transitions were observed relating to their crystalline phases, their storage modulus dropped more dramatically with temperature, indicative of a higher degree of structural anisotropy and poorer dimensional stability with heating.

Only the Bayblend T85 X RE samples were tensile tested due to the failure of the other two materials during the 3D print job. The 3D print of Bayblend had a tensile strength and modulus that were lower than the injection molded reference due to micro-voids and inter-layer anisotropic properties that are typical in the FGF printing process. Nevertheless, these differences, while not trivial, demonstrated that amorphous PC/ABS blends can have sufficient mechanical integrity as long as the printing parameters are properly controlled. The output data confirm that for 3D prints of isotropic thermoplastics, layer adhesion and part uniformity will primarily drive tensile performance.

This comparative study highlighted that to some extent, AM can produce polymer components with comparable thermal and mechanical properties as injection molded parts, particularly when the polymer being used is amorphous and printing parameters are optimized. Bayblend T85 X RE showed minimal thermal degradation, stable viscoelastic behaviour, and adequate mechanical properties to facilitate its use as a 3D printing material. On the other hand, polymers with semi-crystalline morphologies like PA6 and PP, were problematic to print due to their high degree of crystallisation, large shrinkage and melting behaviour that prevents layers from bonding rigidly to one another. Moving forward, a primary target in the future will be developing improved temperature control, adhesion of neighbouring surfaces, and material modification to promote printability. While this study does conclude that 3D printing has the capability of producing polymer components that are not fully comparable to those produced by injection molding, it does provide a robust sustainable and multi-faceted method to produce fully functional engineering polymer components.

BIBLIOGRAPHY

- [1] Jung, S., Lee, J., Kim, H., et al. (2023). Is Additive Manufacturing an Environmentally and Sustainable Alternative? A Review. Sustainability, 15(9), 1–23.
- [2] Al Rashid, A., Khan, S. A., Al-Ghamdi, S. G. (2023). Additive manufacturing for sustainability and circular economy. Materials Today Sustainability, 23, 100216.
- [3] Sardon, H., & Meabe, L. (2022). Sustainable Additive Manufacturing of Plastics. ACS Sustainable Chemistry & Engineering, 10(5), 1759–1774.
- [4] Bilal, E., Smith, J., Martinez, P., et al. (2024). Circularity: Understanding the Environmental Tradeoffs of Additive Manufacturing with Waste Plastics. Recycling, 9(5), 72.
- [5] Jayawardane, H. M., Fernando, M. S., & Bandara, C. (2023). Additive manufacturing of recycled plastics: a techno-eco-efficiency assessment. The International Journal of Advanced Manufacturing Technology, 127, 1–18.
- [6] E. Saldívar-Guerra and E. Vivaldo-Lima, 'Introduction to Polymers and Polymer Types', Handbook of Polymer Synthesis, Characterization, and Processing. John Wiley and Sons, pp. 1–14, Feb. 22, 2013. doi: 10.1002/9781118480793.ch1
- [7] H. F. Brinson and L. C. (L. C. Brinson, Polymer engineering science and viscoelasticity: an introduction. Springer, 2008.
- [8] E. Kabir, R. Kaur, J. Lee, K. H. Kim, and E. E. Kwon, 'Prospects of biopolymer technology as an alternative option for non-degradable plastics and sustainable management of plastic wastes', Journal of Cleaner Production, vol. 258. Elsevier Ltd, Jun. 10, 2020. doi: 10.1016/j.jclepro.2020.120536.
- [9] J. P. Pascault and R. J. J. Williams, 'Thermosetting Polymers', in Handbook of Polymer Synthesis, Characterization, and Processing, John Wiley and Sons, 2013, pp. 519–533. doi:10.1002/9781118480793.ch28.
- [10] Narendra Kumar, Piyush D. Ukey, Vishal Francis, Ravi Pratap Singh, Sonika Sahu, Polymers for 3D Printing Methods, Properties, and Characteristics Plastics Design Library 2022, Pages 307-323
- [11] Michel Biron Thermoplastics and Thermoplastic Composites (Second Edition) Plastics Design Library 2013, Pages 1-29
- [12] Schelleis, C. et al. Approaching Polycarbonate as an LFT-D Material: Processing and Mechanical Properties. Polymers, 2023, 15(9):2041. DOI: 10.3390/polym15092041
- [13] B. Majumdar, D.R. Paul, in: D.R. Paul, C.P. Bucknall (Eds.), Polymer Blends, vol. 2, John Wiley & Sons, New York, 1999.
- [14] D.W. Fox, E.N. Peters, in: R.W. Tess, G.W. Poehlein (Eds.), Applied Polymer Science, second ed., ACS, Washington, DC, 1985, p. 495.

- [15] M. Pagac et al., 'A review of vat photopolymerization technology: Materials, applications, challenges, and future trends of 3d printing', Polymers, vol. 13, no. 4. MDPI AG, pp. 1–20, Feb. 02, 2021. doi: 10.3390/polym13040598.
- [16] R. Chaudhary, P. Fabbri, E. Leoni, F. Mazzanti, R. Akbari, and C. Antonini, 'Additive manufacturing by digital light processing: a review', Progress in Additive Manufacturing, vol. 8, no. 2. Springer Science and Business Media Deutschland GmbH, pp. 331–351, Apr. 01, 2023. doi: 10.1007/s40964-022-00336-0.
- [17] S. Bose, D. Ke, H. Sahasrabudhe, and A. Bandyopadhyay, 'Additive manufacturing of biomaterials', Progress in Materials Science, vol. 93. Elsevier Ltd, pp. 45–111, Apr. 01, 2018. doi: 10.1016/j.pmatsci.2017.08.003.
- [18] L. J. Tan, W. Zhu, and K. Zhou, 'Recent Progress on Polymer Materials for Additive Manufacturing', Advanced Functional Materials, vol. 30, no. 43. Wiley-VCH Verlag, Oct. 01,2020. doi: 10.1002/adfm.202003062.
- [19] C. Noè et al., 'DLP-printable fully biobased soybean oil composites', Polymer (Guildf), vol.247, Apr. 2022, doi: 10.1016/j.polymer.2022.124779.
- [20] S. C. Ligon, R. Liska, J. Stampfl, M. Gurr, and R. Mülhaupt, 'Polymers for 3D Printing and Customized Additive Manufacturing', Chemical Reviews, vol. 117, no. 15. American Chemical Society, pp. 10212–10290, Aug. 09, 2017. doi: 10.1021/acs.chemrev.7b00074.
- [21] Tofail, S.A., Koumulos E.P., Bandyopadhyay A., Bose S., O'Donoghue L., Charitidis C., "Additive manufacturing: scientific and technological challenges, market uptake and opportunities", Materials Today, 21(1), pages 22-37, 2018.
- [22] Sathies, T., Senthil P., Anoop M.S., "A review on advancements in applications of fused deposition modelling process", Rapid Prototypig Journal, 26(4), pages 669-687, 2020.
- [23] Gasman, L., "Additive aerospace considered as a business", Froes F., Boyer R., Additive Manufacturing for the Aerospace Industry, pages 327-340, Elsevier, 2019.
- [24] Wiese, M., Thiede S., Herrmann C., "Rapid manufacturing of automotive polymer series parts: A systematic review of processes, materials and challenges", Additive Manufacturing, 36,101582, pages 1-13, 2020.
- [25] Smith, M.L., Jones F.X.j., "Dual-extrusion 3D printing of anatomical models for education", Anatomical Sciences Education, 11(1), pages 65-72, 2018.
- [26] Ngo, T.D., Kashani A., Imbalzano G., Nguyen K.T.Q., Hui D., "Additive manufacturing (3D printing): A review of materials, methods, applications and challenges", Composites Part B, 143, pages 172-196, 2018.
- [27] Dizon, J.R.C., Esperajr A.H., Chen Q., Advincula R. C., "Mechanical characterization of 3D-printed polymers", Additive Manufacturing, 20, pages 44-67, 2018.
- [28] Das, A., Chatham C. A., Fallon J. J., Zawaski C. E., Gilmer E. L., Williaös C. B., Bortner M. J., "Current understanding and challenges in high temperature additive

- manufacturing of engineering thermoplastic polymers", Additive Manufacturing, 34, 101218, pages 1-21, 2020.
- [29] Daminabo, S., Goel S., Grammatikos S.A., Nezhad H.Y., Thakur V.K., "Fused deposition modeling-based additive manufacturing (3D printing): techniques for polymer material systems", Materials Today Chemistry, 16, 100248, pages 1-23, 2020.
- [30] Leary M.,"Material Extrusion", Design for Additive Manufacturing, Elsevier, pages 223-268, 2020.
- [31] Chohan, J.S., Singh R., "Pre and post processing techniques to improve surface characteristics of FDM parts: a state of art review and future applications", Rapid Prototyping Journal, 23(3), pages 495-513, 2017.
- [32] Lalehpour, A., Janeteas C., Barari, "Surface roughness of FDM parts after post-processing with acetone vapor bath smoothing process", The International Journal of Advanced Manufacturing Technology, 95, pages 1505-1520, 2018.
- [33] J. Jakubiak and J. F. Rabek, 'Three-dimensional (3D) photopolymerization in stereolithography. Part I: fundamentals of 3D photopolymerization.', 2000.
- [34] Covestro AG. Bayblend® T85 X RE Product Datasheet. Covestro Solutions, 2025
- [35] Material Data Center. Bayblend® T85 X RE Technical Data. 2025.
- [36] Tumaker. (2020). *NX 300 Modular Technical specifications*. Tumaker Official Website 2025.
- [37] A. Barkane et al., 'Uv-light curing of 3d printing inks from vegetable oils for stereolithography', Polymers (Basel), vol. 13, no. 8, Apr. 2021, doi: 10.3390/polym13081195.
- [38] A. Lanzotti, G. Grasso, M. Staiano, A. Martorelli, The impact of process parameters on mechanical properties of parts produced in PLA with an open-source 3D printer, Rapid Prototyping Journal, 21(5), 604–617 (2015).
- [39] L. Fontana, F. Lavecchia, A. Frascella, M. Buccoliero, Characterization of 3D Printed Polylactic Acid by Fused Granulate Fabrication (FGF), Polymers, 14(17), 3530 (2022).
- [40] M. Spoerk, R. Holzer, C. Holzer, Material extrusion-based additive manufacturing of polypropylene: A review on how to improve dimensional inaccuracy and warpage, Journal of Applied Polymer Science, 137(12), 48545 (2020).
- [41] B. M. Tymrak, M. Kreiger, J. M. Pearce, Mechanical properties of components fabricated with open-source 3D printers under realistic environmental conditions, Materials & Design, 58, 242–246 (2014).
- [42] A. M. Cárdenas, C. Hopmann, J. Haase, Processing behavior of recycled polymers in pellet extrusion 3D printing: Influence on mechanical and thermal properties, Additive Manufacturing, 55, 102891 (2022).